Ultrasonics Sonochemistry 117 (2025) 107339

Contents lists available at ScienceDirect

Ultrasonics Sonochemistry

journal homepage: www.elsevier.com/locate/ultson

Anti-inflammatory and gut microbiota regulatory effects of ultrasonic degraded polysaccharides from *Auricularia auricula-judae* in DSS-induced colitis mice

Tahidul Islam [a,b], Baojun Xu [c,*], Zhaoxiang Bian [a,b,*]

[a] Centre for Chinese Herbal Medicine Drug Development Limited, Hong Kong Baptist University, Hong Kong SAR, China
[b] School of Chinese Medicine, Hong Kong Baptist University, Hong Kong SAR, China
[c] Food Science and Technology Program, Department of Life Sciences, Beijing Normal-Hong Kong Baptist University, China

ARTICLE INFO

Keywords:
A. auricula-judae
Polysaccharide
Ultrasonic degradation
Physiochemical properties
Anti-inflammatory effects
Gut microbiota effects

ABSTRACT

Auricularia auricula-judae is a widely cultivated mushroom species known for its edible and medicinal properties. Polysaccharides have been the focus of research because of their potential bioactivities; nonetheless, the structural complexity and molecular weight have hindered a complete understanding of their bioactivities. In this study, AP-1 polysaccharide was isolated from *A. auricula-judae* and subjected to ultrasonic degradation at different time points to improve their anti-inflammatory effects. The results showed that when AP-1 was degraded for 9 min (AP-2) and 20 min (AP-3), the NO inhibition rate was significantly increased in LPS-stimulated RAW 264.7 cells. The structural and physiochemical properties of native and degraded polysaccharides were analyzed, and it was found that the degradation process significantly reduced molecular weight and altered the particle size, viscosity, crystallinity, and helical structure. Furthermore, native and degraded polysaccharides (AP-1, AP-2, and AP-3) anti-inflammatory effects were investigated in the DSS-induced colitis mouse model. Degraded polysaccharides resulted in significant improvements, including recovery from weight loss, reduced disease activity, shortened colon length, and decreased inflammation, while AP-3 showed the most promising effects. Gut microbiota 16S rRNA sequencing revealed that AP-3 potentially increases healthy gut microbiota and inhibits unhealthy gut microbiota. Overall, this study demonstrates that ultrasonic degradation could be a great technique to modify polysaccharides' MW and physiochemical properties to improve anti-inflammatory and gut microbiota regulatory effects.

1. Introduction

A. auricula-judae is one of the most popular edible and medicinal mushrooms with numerous health-promoting benefits [27]. In most Asian countries, *A. auricula-judae* mushrooms are grown in large amounts, while it is the fourth largest cultivated mushroom globally due to their high demand. Its high consumption is attributable to its taste, soft texture, flavor, nutritional value, and health-promoting chemical composition [28]. Polysaccharides are one of the major active components in the fruiting body of *A. auricula-judae*, which promote antioxidant, antitumor, anticoagulant, and antifatigue effects, while its molecular weight is relatively higher [11,49,55]. A previous study reported that a β-glucan polysaccharide from *A. auricula-judae* mushroom has a higher molecular weight of 1200 kDa [64]. Mushroom polysaccharides have gained much popularity in recent years for their widespread use in a variety of industrial applications and their wide range of pharmacological and biological effects, including anti-inflammatory effects.

Inflammatory bowel disease (IBD) is a chronic inflammation of the digestive system, while Crohn's disease and ulcerative colitis (UC) are the two main types of IBD. Nowadays, UC is a severe problem due to an unhealthy lifestyle, unhealthy food consumption, smoking, drinking alcohol, and gut microbial dysbiosis. The intestinal tract is affected, causing diarrhea, abdominal pain/cramping, blood in stool, fatigue, fever, weight loss/anorexia, loss of appetite, and increased risk of colon cancer [33,43,84]. In recent studies, researchers have focused more on

* Corresponding authors at: 2000 Jintong Road, Tangjiawan, Zhuhai, Guangdong 519087, China (B. Xu). Jockey Club School of Chinese Medicine Building, 7 Baptist University Road, Kowloon Tong, Hong Kong SAR, China (Z. Bian).
E-mail addresses: baojunxu@uic.edu.cn (B. Xu), bzxiang@hkbu.edu.hk (Z. Bian).

https://doi.org/10.1016/j.ultsonch.2025.107339
Received 18 January 2025; Received in revised form 21 March 2025; Accepted 31 March 2025
Available online 1 April 2025

natural compounds, especially polysaccharides, for treating IBD, as synthetic drugs have shown side effects. However, the bioactivities of polysaccharides are often associated with their chemical structure, monosaccharide composition, molecular weights, helical structure, degree of branching, particle size, solubility, and other factors [19,28,65]. Previous studies have reported that high MW polysaccharides have higher bioactivities [14], but the structural complexity of these polysaccharides often limits the proper utilization of their bioactivities in our bodies and remains unknown their optimum efficacy. The high molecular weight polysaccharides cannot penetrate numerous cell membrane barriers into our body to exert pharmacological effects and cannot be wholly fermented or degraded by the gut microbiota in the gut [3,41]. High MW, poor solubility, and high viscosity are some obstacles preventing polysaccharides from being widely used in the pharmaceutical and food sectors.

Moreover, lower MW compounds are demanded in many unique applications, especially in the cosmetics and pharmaceuticals industry, due to the advantage of improving diffusion into bloodstreams and biological tissues [25]. Degradation of polysaccharides is an excellent technique to alter their MW and physiochemical properties (particle size, viscosity, helical structure, crystallinity, and solubility), thereby improving their bioactivities and breaking the complexity of their application in the pharmaceutical and food industries. Chemical, enzymatic, and physical (ultrasonic treatment) methods are widely popular for the degradation of polysaccharides [86]. However, chemical methods require large amounts of organic reagents, high temperatures, time-consuming, and cause environmental pollution [20,81]. In contrast, enzymatic methods are costly and greatly restrict their application on an industrial scale. On the other hand, ultrasonic degradation is an effective, efficient, and environmentally friendly method for polysaccharide degradation, which has received significant attention recently [19,45]. However, the anti-inflammatory and gut microbiota regulating effects and the underlying mechanisms of degraded *A. auricula-judae* polysaccharides in colitis mice are still unclear. Therefore, this study aims to investigate the degraded *A. auricula-judae* polysaccharides and analyze whether the modified structure is associated with the function, especially in terms of its anti-inflammatory and gut microbiota regulatory efficacy.

In this study, *A. auricula-judae* mushroom polysaccharide was isolated and degraded by an ultrasonic cell disruptor at different time points to improve its anti-inflammatory efficacy, which was monitored by the NO inhibitory rate using LPS-stimulated RAW 264.7 cells. Native and two degraded polysaccharides were selected to examine their physicochemical characteristics in relation to their anti-inflammatory effects. Furthermore, native and degraded *A. auricula-judae* polysaccharides were administered to DSS-induced colitis mice to investigate their anti-inflammatory effects by analyzing histological changes, mucin expression, and inflammatory cytokines secretion in the colon. The higher anti-inflammatory effects among these three polysaccharides were further investigated by examining the protein expression of iNOS, COX-2, and NF-κBs in the colon. In contrast, the gut microbiota regulatory effects were observed in mice fecal samples by 16S rRNA gut microbiota sequencing.

2. Materials and methods

2.1. Chemicals, reagents, and sample collection

Slide-A-Lyzer™ Dialysis flask (MWCO 3.5 kDa) was purchased from ThermoFisher Scientific, Waltham, Massachusetts, U.S.A. Dialysis membrane (MWCO 6–8 kDa), Spectrum® Laboratories, Song Jiang District, Shanghai, China. Lipopolysaccharides from *Escherichia coli* O111:B4 (LPS) L2630-25MG, muscovite mica for AFM (AFM-71856–02), dextran standard, (Molecular weight: 1000, 5000, 25000, 50000, 270000, 410000, 650000 Da), congo red (C6767-25G), deuterium oxide (D_2O, 7789–20-0), D-(+)- mannose (3458–28-4), D-(+)-arabinose (5328–37-0), D-(+)-galactose (59–23-4), D-(+)-glucose (50–99-7), L-rhamnose (10030–85-0), D-(+)-fucose (3615–37-0), and D-gluconic acid solution (526–95-4) were purchased from Sigma-Aldrich, Merck Limited, Shanghai, China. Tianjin Damao Chemical Reagent Co., Ltd. (Tianjin, China) supplied the remaining chemicals and reagents. All chemicals were of analytical grade unless specially mentioned. Dextran sulfate sodium (colitis grade, MW 36,000–50,000 Da) was purchased from MP Biomedicals, California, U.S.A. Griess reagent kit (G7921) and 5-aminosalicylic acid (89–57-6) were purchased from ThermoFisher Scientific, Waltham, Massachusetts, U.S.A. Mouse ELISA kits TNF-α (EM008-96), IL-1β (EM001-96), and IL-6 (EM004-96) were purchased from Shanghai Jitai Yikesai Biotechnology Co., Ltd, Shanghai, China. Primary antibody iNOS (ab204017) was purchased from Abcam (Hong Kong) Limited, Hong Kong SAR, China; COX-2 (12282S), Nrf-2 (12721S), and NFκB p65 (8242S) were purchased from Cell Signaling Technology, Danvers, Massachusetts, U.S.A; mouse anti-ZO-1(339100) and loading control (MA515738D680) were purchased from ThermoFisher Scientific, Waltham, Massachusetts, USA; p-NFκB p65 (sc-166748), IκB-α (sc-1643), p-IκB-α (sc-8404), and secondary antibodies mouse anti-rabbit IgG-HRP (sc-2357) and m-IgGκ BP-HRP (sc-516102) were purchased from Santa Cruz Biotechnology, California, U.S.A. Dry *A. auricula-judae* mushroom was collected from the College of Horticulture, Jilin Agricultural University, Changchun 130118, China.

2.2. Extraction, isolation, and purification of A. auricula-judae polysaccharide

The extraction of *A. auricula-judae* crude polysaccharide was carried out in accordance with the method outlined by Zhang et al. [82], and Zhang et al. [83] with some modifications including overnight incubation with absolute ethanol (extract: ethanol 1:3) at 4 °C. After being separated by centrifugation, the precipitated polysaccharide was lyophilized. The sevag method was applied to a 2 % crude polysaccharides solution for the removal of proteins [50], then the pH was adjusted to 8.0 with ammonia, and color pigments were removed by adding 3 % of H_2O_2 according to the procedure described by Xiong et al. [77] and lyophilized. Polysaccharide was redissolved and eluted through DEAE–52 columns (2.7 cm × 70 cm) with distilled water and 0.2–1.0 M NaCl solutions to collect the fractions at a flow rate of 0.2 mL/min (each test tube was held for 18 min) and was monitored by using the phenol–sulfuric acid method. The major polysaccharide fraction was concentrated using a rotary evaporator and named AP-1. The concentrated AP-1 was dialyzed using MWCO 3.5 kDa and 6–8 kDa dialysis membranes against DDI water for 48 h and 72 h. Finally, the purified polysaccharide extract was lyophilized, and the total polysaccharide content was measured by the phenol–sulfuric acid method. The extraction flowchart is presented in Fig. 1A.

2.3. Determination of monosaccharides composition of AP-1 A. auricula-judae polysaccharides

The monosaccharides composition of AP-1 polysaccharides was determined using the methods outlined by Li et al. [40] with slight modifications. Monosaccharides were analyzed by HPLC-DAD. At 120 °C for 2 h, 2 mol/L TFA was used to hydrolyze polysaccharides of varying molecular weights. The hydrolyzed polysaccharides were redissolved in methanol after being completely dried and with TFA removed, then the supernatant was filtered through a 0.45 μm membrane and transferred into 1.5 mL HPLC vials. Standard solutions of glucose, mannose, galactose, arabinose, fucose, and rhamnose were prepared by dissolving them in methanol to provide a range of concentrations for use in fitting the external calibration curve. The HPLC-DAD detector and Shodex Asahipak NH2P-50 4E column (4.6 mm ID × 250 mm) were used. The sample volume was 20 μL, and mobile phases A and B (water and acetonitrile) were employed at a column temperature of 30 °C. At a flow rate of 1 mL/min, 90 % of mobile phase B was

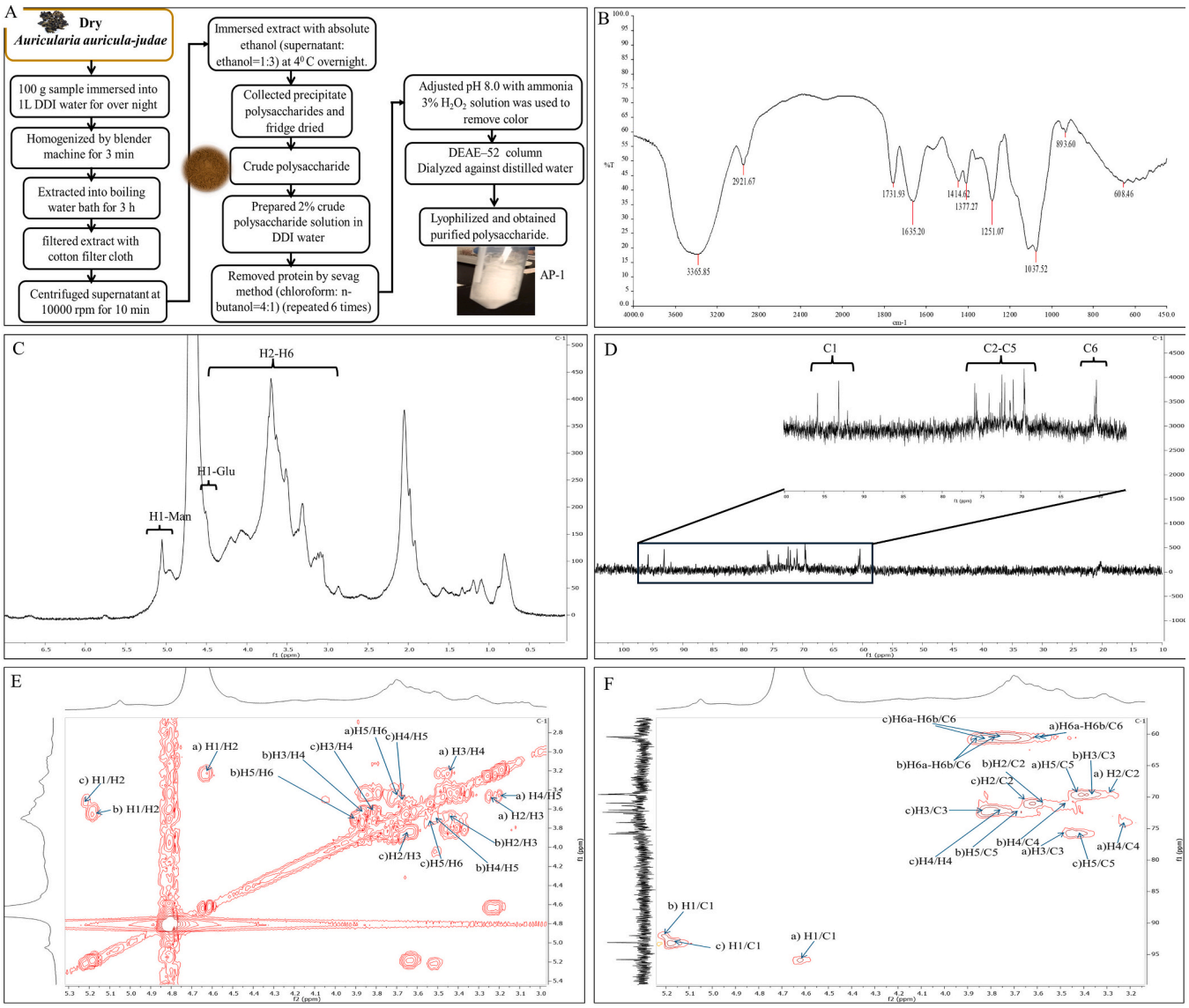

Fig. 1. *A. auricula-judae* polysaccharides extraction and structural analysis. (A) AP-1 polysaccharide was isolated according to this flowchart: (B) FT-IR spectrum; (C)^{1}H NMR spectrum (D) ^{13}C NMR spectrum; (E) COSY NMR spectrum; (F) HSQC NMR spectrum.

used from 0 to 30 min, and 20 % from 30.1 to 40 min.

2.4. NMR structural analysis of AP-1 A. auricula-judae polysaccharides

AP-1 polysaccharides (about 20 mg) were dissolved in 400 μL D_2O and afterwards transferred to an NMR test tube. At 25 °C, the ^{1}H NMR and ^{13}C NMR spectra were measured using a Bruker Avance III 400 spectrometer. Standard Bruker software and Mestre Nova were used to process the data, and the chemical shifts for ^{1}H and ^{13}C NMR were reported in ppm.

2.5. Infrared (IR) spectrum measurement of AP-1 A. auricula-judae polysaccharides

AP-1 polysaccharide powder (about 5 mg) was mixed with the potassium bromide (KBr) powder (weighing about 200 mg), then both were finely crushed using a mortar and pestle before being dried at 50 °C for 10 min. The powder was then compressed into 1 mm pellets, and a TENSOR 27 fourier transform infrared (FT−IR, Bruker Corporation, Karlsruhe, Germany) spectrophotometer was used to determine the IR spectra in the frequency range from 4000 to 400 cm^{-1}.

2.6. Degradation of A. auricula-judae polysaccharide by ultrasonic cell disruptor

The SM-1000A ultrasonic cell disrupter (Nanjing Shunma Instrument Equipment Co., Ltd., Nanjing, China), at 25 kHz frequency with a maximum output power of 1000 W, was used to degrade the polysaccharide. The AP-1 polysaccharide was dissolved in water (4 mg/mL), and a probe with a 12 mm tip was used. The power was adjusted to 600 W, the on/off time was set to 5/2 s, then the polysaccharide was degraded at different time periods (9 min, 20 min, 40 min, and 60 min). The polysaccharide solution in a beaker was placed in an ice water bath to keep the temperature lower, and solutions were stirred for a few seconds in 3-minute intervals throughout the ultrasonic. The degraded polysaccharides were then lyophilized and stored at −80 °C for further study. Two different degradation time points were screened and selected based on their NO inhibition rates in LPS-stimulated RAW cells for further study.

2.7. Determination of molecular weight (MW) of native and degraded A. auricula-judae polysaccharides

The MW of AP-1 and degraded *A. auricula-judae* polysaccharides were determined using the methods outlined by Li et al. [40]. MW was determined using HPGPC-DAD dictator. Under the same experimental condition used to establish the molecular weight-retention time calibration curve, the different molecular-weight dextran (1, 5, 12, 25, 50, 80, 150, 270, 410, and 670 kDa) aqueous solutions were injected into the HPGPC-CAD.

2.8. Viscosity analysis of native and degraded A. auricula-judae polysaccharides

Using an LV DV-II + Pro viscometer, the viscosity of native and degraded *A. auricula-judae polysaccharides* solutions was determined (Brookfield Company, Stoughton, MA, U.S.A.). Polysaccharides were diluted to a concentration of 4 mg/mL in deionized water. The viscosity cP value of *A. auricula-judae* polysaccharides was measured at 25 °C using a spindle 62 with a speed range of 0.5 to 100 rpm.

2.9. Particle size distribution analysis of native and degraded A. auricula-judae polysaccharides

The native and degraded *A. auricula-judae* polysaccharides were dissolved in distilled water at a concentration of 0.01 mg/mL, then the DelsaTM Nano HC particle analyzer was used to measure the distribution of polysaccharides particle size (Beckman Coulter, U.S.A.).

2.10. SEM and EDX analysis of native and degraded A. auricula-judae polysaccharides

The native and degraded *A. auricula-judae* polysaccharides were - studied by scanning electron microscopy and energy dispersive X-ray analysis using an LEO 1530 Field Emission SEM microscope (LEO company, Germany) at 10 kV acceleration. For scanning electron microscopy analysis of the polysaccharides, their fracture surfaces were gold-vacuum coated for morphological and elemental characterization.

2.11. X-ray diffraction (XRD) analysis of native and degraded A. auricula-judae polysaccharides

Native and degraded *A. auricula-judae* polysaccharides powder was mounted onto a glass slide sample holder and aligned. The XRD measurement was carried out using Bruker AXS D8 Advance X-Ray Diffractometer.

2.12. AFM analysis of native and degraded A. auricula-judae polysaccharides

The native and degraded *A. auricula-judae* polysaccharides were examined using atomic force microscopy (AFM) in a manner similar to that reported by Wang et al. [71] with some modifications. Polysaccharides solution was prepared in distilled water at a concentration of 0.01 mg/mL, and 20 μL was applied to the surface of the muscovite mica (Sigma) sample carrier. The polysaccharides on the mica sample were fixed by dripping absolute ethanol onto the sample. Following this, double-distilled water and air were used to blow the sample carrier, and AFM images were obtained from Nano Magnetics, ezAFM + KPFM (Nano Magnetics Instruments Ltd., United Kingdom).

2.13. Anti-inflammatory activity analysis of native and degraded A. auricula-judae polysaccharides in RAW 264.7 cells

2.13.1. Cell culture

RAW 264.7 cells were cultured in a humidified incubator with 5 % CO_2 at 37 °C, using DMEM supplemented with 10 % FBS, 100 U/mL penicillin, and 100 μg/mL streptomycin.

2.13.2. MTT assay

The MTT assay was used to evaluate cell viability. RAW264.7 cells, at a density of 1.2 x 10^4 cells per well, were seeded into a 96-well plate, and the plate was incubated with 5 % CO_2 at 37 °C overnight. The cells were then pre-treated with different doses of native and degraded *A. auricula judae* polysaccharides (50, 100, 200, 400, and 800 μg/mL in medium) for 2 h prior to the addition of LPS (1 μg/mL). After 24 h of incubation in a humidified incubator with 5 % CO_2 at 37 °C, 500 μg/mL of MTT solution was added for an additional 3 h of incubation. After discarding the supernatant, 100 μL DMSO was added to each well to dissolve the formazan. A microplate reader was used and set to 570 nm to measure absorbance. The proportion of living cells was compared to the Control.

2.13.3. Determination of NO production

RAW264.7 cells were seeded into 24-well plates (8×10^4 cells per well) overnight and then pre-treated with AP-1, AP-2, AP-3, AP-4, and AP-5 polysaccharides at different concentrations (50, 100, and 200 μg/mL) for 2 h prior to the addition of LPS (1 μg/mL). After 18 h of incubation in a humidified incubator with 5 % CO_2 at 37 °C, the medium was collected, and the quantity of NO release was quantified using the Griess reagent kit (ThermoFisher) in accordance with the manufacturer's instructions. Nitrite was used to prepare external standards at varying concentrations (4–100 μM). The percentage of NO production inhibition rate was calculated based on the LPS group as 100 % control. The cells only treated with LPS were used as LPS, whereas untreated cells were used as Control. The NO production inhibition rate was calculated according to the following formula.

NO inhibition (%) = 100 x [1 – (LPS – Control) / (LPS – Control)].

2.14. Animals

Male C57BL/6J mice (aged five to six weeks and weighing 20–24 g) were acquired from the Laboratory Animal Services Centre of the Chinese University of Hong Kong. The mice were given conventional mouse food with unrestricted access to water and were housed in rooms maintained at 22 ± 1°C with 12 h light/dark cycle at the Hong Kong Baptist University Animal facility under specific pathogen-free (SPF) conditions. All animal experiments followed the Animal Ordinance Guidelines, Department of Health, Hong Kong SAR ((22–22) in DH/HT&A/8//2/6Pt.5).

2.15. Induction of colitis and treatments

Mice were randomly divided into nine groups (N = 7): Control, DSS, Positive Control, AP-1 LD, AP-1 HD, AP-2 LD, AP-2 HD, AP-3 LD, and AP-3 HD. Colitis was induced by DSS administration, as described previously, with some modifications [16]. Briefly, colitis was induced by feeding DSS water in three cycles; in the first cycle, 2 % of DSS water was given for six days (day 0–6); in the second cycle, 1.7 % of DSS water was given for five days (day 13–18); and in the third cycle, 1.7 % of DSS water was given for five days (day 25–30). Except for three cycles of DSS water, mice received normal drinking water during the whole experimental period. From day 13, the different groups of mice were orally administered the corresponding drugs, such as Positive Control (5-ASA 50 mg/kg b.w.), AP-1 LD (AP-1 125 mg/kg b.w.), AP-1 HD (AP-1 250 mg/kg b.w.), AP-2 LD (AP-2 125 mg/kg b.w.), AP-2 HD (AP-2 250 mg/kg b.w.), AP-3 LD (AP-3 125 mg/kg b.w.), and AP-3 HD (AP-3 250 mg/kg b.w.). The body weights of all the mice were recorded three times each week, and the disease activity index (DAI) was assessed at a specified time point throughout the experimental treatment period. The evaluation of the DAI score was done with the standard parameters as described in Table 1. To analyze the 16S rRNA gut microbiota sequencing, fecal samples were collected on day 30 and stored at

Table 1
Disease Activity Index (DAI).

Parameters	Score	Description
Changes in body weight	0	Gained b.w./Remain the same
	1	Lost 1–5 % of original bodyweight
	2	Lost 6–10 % of original bodyweight
	3	Lost > 10 % of original bodyweight
Fecal occult blood (Twice in a week)	0	Occult blood absent
	1	Occult blood detected
	2	Bloodstains in feces
	3	Significant bleeding in feces
Fecal consistency (Twice in a week)	0	Normal feces
	1	Soft feces
	2	Mild diarrhea
	3	Severe diarrhea

−80 °C. On day 31, the mice were sacrificed, and blood samples were collected from their hearts using a heparin-filled 2 mL syringe. The blood was immediately centrifuged at 15000 rpm for 10 min at 4 °C, and the resulting blood serum was collected and stored at −80 °C until further analysis. After removing the colon, their lengths were measured and documented. Fecal samples were removed from the colon and washed with PBS, and 1 cm of the distal end of each colon was taken and stored in 4 % PFA for further histopathology and immunohistochemical assays. The remaining colon was stored at −80 °C for biochemical study. Afterwards, the heart, kidney, liver, lung, and spleen were collected, and their weights were measured. All the tissues were rinsed with PBS and stored at −80 °C for further analysis.

2.16. Colon tissue processing for histopathology and immunohistochemistry analysis

Distal colon samples were harvested and washed with PBS. The distal colon (1 cm) was immediately cut and preserved in 4 % PFA for 48 h. Afterward, the tissue was placed in a 30 % sucrose solution and stored at 4 °C. By using the previously established cryosection procedures, the colon tissue was sectioned at a thickness of 15 μm [22]. The tissue sections were stored at 4 °C in 0.4 % PBST for histopathology and immunohistochemistry analysis.

2.17. H&E and alcian blue staining

The various groups of colon tissue sections were placed on microscope glass slides and dried at 37 °C. The slides were then stained with hematoxylin and eosin (H&E) stains following the manufacturer's instructions. For apparent mucin staining, alcian blue was stained according to the manufacturer's procedure (IHC WORLD, LLC, U.S.A.), with minor adjustments to substitute neutral red with eosin. Leica (DMI 3000B) microscope images of H&E and alcian blue stained sections were captured. The histological scoring was conducted in accordance with the report by Winter et al. [73], and Xiao et al. [76] with slight adjustments. ImageJ software was used to quantify the intensity of the alcian blue staining.

2.18. Determination of inflammatory cytokines in blood serum and colon tissue by ELISA

A colon tissue piece weighing around 20 mg was lysed with 500 μL PBS in a tissue homogenizer for 5 min. The tubes were centrifuged at 15,000 rpm for 10 min, and the supernatant was transferred to a fresh set of 2 mL tubes. The BCA method was used to measure total protein content, and 1X PBS was used to equalize the total protein concentration of each sample. In accordance with the manufacturer's instructions, mouse ELISA kits were used to measure inflammatory cytokines in the supernatant (Shanghai Jitai Yikesai Biotechnology Co., Ltd, Shanghai, China). Mouse ELISA kits were used to measure TNF-α in mouse blood serum according to the manufacturer's instructions.

2.19. Immunohistochemistry analysis

The free-floating sections were used for immunostaining. The colon tissue section was taken and washed with 1X PBST and blocked with a blocking solution (5 % BSA in 1X PBST) for 2 h at room temperature. The tissue sections were then washed twice with 1X PBST and incubated with diluted primary antibody overnight at 4 °C. The next day, tissue sections were washed twice, followed by incubation with secondary antibody at 4 °C for 2 h. Sections were washed with 1X PBST and mounted with a DAPI containing mounting media. Confocal Laser Scanning Microscope Leica was used to capture immunofluorescence images of the colon tissue section (TCS SP8). Images were analyzed and quantified using ImageJ software.

2.20. Western blotting

Colon tissues were lysed in RIPA buffer containing phosphatase inhibitor cocktail (ThermoFisher Scientific, U.S.A.) and homogenized for 5 min. After 10 min of centrifugation at 15,000 rpm, the supernatant was collected, and the total protein content was determined using the BCA method. The protein content was normalized, then combined with 4 × loading buffer and heated at 95 °C for 7 min. The samples were analyzed by western blotting according to the protocol described by Abcam and then incubated with HRP-conjugated anti-rabbit/anti-mouse IgG antibody. The chemiluminescent substrate (ThermoFisher Scientific, U.S.A.) was added to the membrane to expose the signal and developed on a CL-exposure film. The images were collected using an EPSON scanner, and ImageJ was used to quantify the intensity of the protein bands.

2.21. Fecal sample DNA extraction and 16S rRNA sequence analysis

Three groups of mice fecal samples were selected (Control, DSS, and AP-3 HD groups) for gut microbiota analysis.

According to the manufacturer's instructions, DNA was isolated from fecal samples using the QIAamp DNA stool extraction kit (Qiagen, Germany). The whole genomic DNA was then analyzed by agarose gel electrophoresis at 1 % concentration. A Qubit 2.0 Fluorometer was used to measure the quantity of each sample (ThermoFisher Scientific, Massachusetts, U.S.A.).

For PCR amplification of the 16S rRNA gene's hypervariable V3-V4 region, samples utilized the 338F and 806R universal primers. The amplicon products were purified using AMPure XP beads (Beckman Coulter, Milpitas, U.S.A.). The TruSeq® DNA PCR-free sample preparation kit (Illumina, U.S.A.) was used to create sequencing libraries following the manufacturer's instructions. Agilent Bioanalyzer 2100 was used to evaluate the library's quality (Agilent Technologies, U.S.A.). Finally, high-quality libraries were sequenced using a 250 bp paired-end read Illumina HiSeq 2500 platform. FLASH program (v1.2.7) was used to overlap and combine paired-end readings to get raw tags. Low-quality raw tags were filtered out using Trimmomatic (v0.33) to preserve high-quality clean tags. The program Quantitative Insights Into Microbial Ecology 2 (QIIME2 version 2018–8) was then used, and the clean tags were entered into it [8]. Raw data were sorted into the same operational taxonomic unit as those that shared at least 97 % of their characteristics (OTU). The bacterial taxonomy and diversity were examined using the OTU table. To identify the biomarkers of the microbiota's composition and community functions, a threshold logarithmic Linear Discriminant Analysis (LDA) was carried out.

2.22. Statistical analysis

SPSS 20 and GraphPad Prism were used for statistical analysis and graph preparation. One-way ANOVA and Duncan's novel multiple-range tests were used to determine statistical significance, $p < 0.05$, and the data are presented as mean ± SD.

3. Results and discussion

3.1. Isolation, MW, monosaccharides, and structural elucidation of AP-1 (native) A. auricula-judae polysaccharides

A. auricula-judae AP-1 polysaccharide was extracted according to the flowchart in Fig. 1(A), which was found to be 86.83 % of polysaccharide content after lyophilization. The average molecular weight was found to be 1091 kDa, while glucose (54.27 %) and mannose (29.44 %) were the major monosaccharides, along with minor amounts of fucose (1.60 %), arabinose (8.87 %), and galactose (5.82 %).

Fig. 1(B) displays the FT-IR spectrum of AP-1 *A. auricula-judae* polysaccharides obtained using an FT-IR spectrophotometer, which revealed the characteristics of carbohydrate patterns. The strong, wide characteristic band at 3365.8 cm^{-1} suggested the existence of OH stretching in hydrogen bonds, which was suggestive of the polysaccharide chains' strong intermolecular and intramolecular interactions [67]. The weak band at 2921.67 cm^{-1} was found to be associated with C-H stretching and bending vibrations. The peaks at 1731.9 cm^{-1} and 1251 cm^{-1} were represented by the stretching vibrations of carboxylate groups (C=O) and CeO in the ester group, which indicated the presence of uronic acid [70], while the stretching vibration of C=O in carbonyl groups were observed around at 1635.30 cm^{-1} [29]. The absorbance peaks around 1400–1300 were assigned to the vibrations of CeH and of CH_2 groups [68], while the absorbance peaks at 1200–1000 cm^{-1} were assigned to the contribution of CeOH or CeOeC stretching vibration [44]. The pronounced peak at around 890 cm^{-1} was β-configurations in fractions [56]. Infrared (IR) spectroscopy is a well-established method that has been extensively used in polysaccharide structural investigation [26].

We further elucidated the structure of AP-1 polysaccharides using 1D (^1H and ^{13}C) and 2D (HSQC and COSY) NMR analysis. The glucose residue exhibited an anomeric proton signal at 4.62 ppm and a corresponding carbon signal at 95.93 ppm in the ^1H and ^{13}C NMR spectra, indicative of a β-configuration. A downfield shift was observed at C3 (75.80 ppm) and its corresponding proton signal at 3.42 ppm, confirming substitution at this position. Other carbons, including C2 (69.79 ppm), C4 (74.14 ppm), and C5 (69.63 ppm), showed no significant shifts, indicating no additional substitutions. The signals for H6a/b (3.65 and 3.54 ppm) and C6 (60.56 ppm) confirmed the presence of a free primary hydroxyl group, consistent with a β-(1 → 3)-linked glucose backbone, a feature commonly observed in fungal β-glucans [38]. The mannose residue (residue b) displayed an anomeric proton signal at 5.20 ppm and a corresponding carbon signal at 92.01 ppm, indicative of an α-configuration. Substitution at C3 was confirmed by a downfield shift to 69.80 ppm for C3 and 3.30 ppm for H3. The remaining carbons, including C2 (71.41 ppm), C4 (71.29 ppm), and C5 (72.22 ppm), showed no significant shifts, suggesting an α-(1 → 3) glycosidic linkage for this mannose residue. The data are consistent with structural features of fungal mannose-rich polysaccharides [60]. Another mannose exhibited an anomeric proton signal at 5.18 ppm and an anomeric carbon signal at 93.25 ppm, confirming an α-configuration. Substitution at both C3 (71.26 ppm for C3 and 3.84 ppm for H3) and C4 (75.80 ppm for C4 and 3.42 ppm for H4) was observed, suggesting a branching point with α-(1 → 3,4) linkages. This structure is consistent with the typical branching observed in fungal polysaccharides with mannose side chains [60,61]. These data suggested that AP-1 has a β-(1 → 3)-linked glucose backbone with α-(1 → 3)-linked mannose side chains and branching through α-(1 → 3,4) linkages.

3.2. Effects of ultrasonic degradation on NO inhibition and MW of polysaccharides from A. auricula-judae

AP-1 polysaccharides was degraded by an ultrasonic cell disruptor at various time periods, and prepared AP-2 and AP-3 degraded polysaccharides, as illustrated in Fig. 2(A). Chemical, enzymatic, and

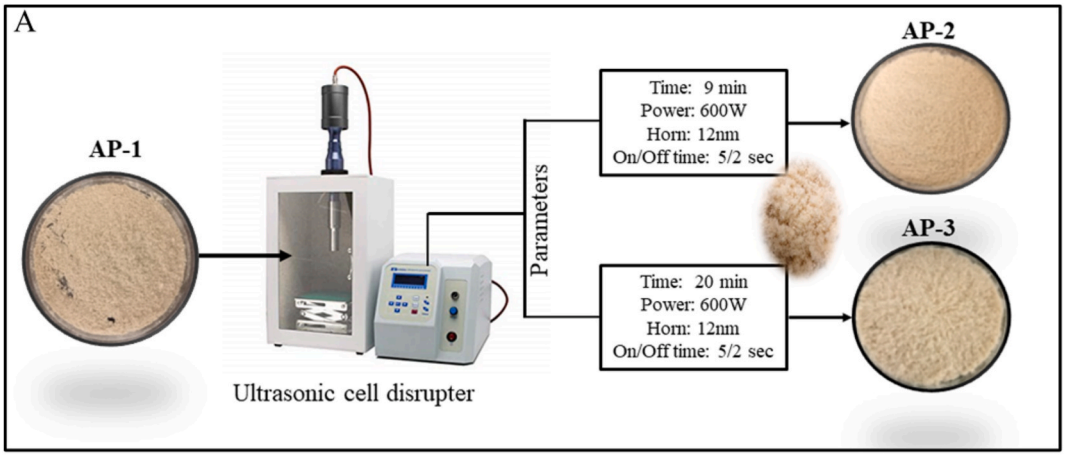

B AP-1, AP-2, and AP-3 polysaccharides NO inhibition rate in LPS stimulated RAW 264.7 cells and their molecular weight

Sample ID	NO inhibition (%)	Molecular weight (kDa)
AP-1	43.09±11.64^{ab}	1091
AP-2	55.24±10.78^{ab}	774
AP-3	68.50±8.50^{a}	326

Fig. 2. Ultrasonic degradation of AP-1 polysaccharide suppressed NO inhibition rates in LPS stimulated RAW 264.7 cells at the concentration of polysaccharides 200 μg/mL while reducing the molecular weights. (A) AP-1 was subjected to ultrasonic degradation at different times and parameters, producing AP-2 and AP-3 (B). The NO inhibition rates were increased in AP-2 and AP-3 polysaccharides while their molecular weight was reduced as compared to the original AP-1 polysaccharides.

physical (ultrasonic treatment) methods are widely popular for the degradation of polysaccharides [86]. However, chemical methods require large amounts of organic reagents and high temperatures, are time-consuming, and are environmentally polluting. [20,81]. In contrast, enzymatic methods are costly and greatly restrict their application on an industrial scale. On the other hand, ultrasonic degradation is an effective, efficient, and environmentally friendly method in polysaccharide degradation, which leads to improved anti-inflammatory effects and has received significant attention recently [19,45]. Ultrasonic degradation of polysaccharides leads to reduced molecular weights, particle size, and viscosity, thereby increasing solubility to enhance its optimum bioactivity [75]. Therefore, we have applied ultrasonic methods to degrade the polysaccharides in our current study to investigate the enhancement of the anti-inflammatory activity of this polysaccharide.

The native and degraded polysaccharides' anti-inflammatory effects were measured by NO inhibitory activity in LPS-stimulated RAW 264.7 cells. MTT assay revealed no cytotoxicity in the cells until the concentration of 200 μg/mL of all polysaccharides, and the NO inhibition activity of native and different degraded *A. auricula-judae* polysaccharides at 200 μg/mL concentration in LPS stimulated RAW 264.7 cells are shown in Fig. 2 (B). The native polysaccharide (AP-1) NO inhibition rate was 43.09 %, whereas degraded polysaccharides of AP-2 (9 min) and AP-3(20 min) NO inhibition rates were at 55.24 % and 68.50 %. In comparison to AP-1, the NO inhibition rates were dramatically increased in AP-2 and AP-3. However, we also degraded the polysaccharide for 40 min and 60 min, during which their NO inhibition rates were no significant compared to the 20-minute (AP-3) degradation. Therefore, native AP-1, and degraded AP-2 and AP-3 were selected for our study. The molecular weight of the degraded AP-2 and AP-3 polysaccharides revealed that AP-2 (774 kDa) and AP-3 (326 kDa) had significantly reduced molecular weights, which is likely an important factor contributing to the improved anti-inflammatory activity. Nitric oxide (NO) is a signaling molecule essential for inflammation-mediated pathogenesis and has anti-inflammatory effects under normal physiological conditions. Excessive NO production in abnormal conditions could turn into a pro-inflammatory mediator that promotes inflammation [2]. There are three types of nitric oxide synthases (NOS) known as endothelium NO synthase (eNOS), neural NO synthase (nNOS), and inducible NO synthase (iNOS) [37]. The nitric oxide synthases (NOS) isoforms are expressed continuously and release NO at low levels, which are important for regular physiological processes. Conversely, inducible nitric oxide synthase (iNOS) generates a large amount of NO under inflammatory stimuli[34]. Lipopolysaccharide (LPS) is a major component of the cell membrane of gram-negative bacteria and is known to induce inflammation [59]. When LPS activates macrophages, they produce a variety of pro-inflammatory cytokines and nitric oxide (NO) through the activation of iNOS. [30]Therefore, the inhibition of NO production in LPS-stimulated RAW 264.7 cells is a well-established method for screening different anti-inflammatory drugs [7,36,80], and the mechanisms of LPS-induced inflammation by excessive NO production is illustrated in Fig. 3. Based on this finding, the physiochemical characteristics and anti-inflammatory effects of AP-1, AP-2, and AP-3 were further investigated.

3.3. Effects of ultrasonic degradation on the viscosity and particle size distribution of *A. auricula-judae* polysaccharide

The native and degraded *A. auricula-judae* polysaccharides' viscosity was analyzed, and the viscosity graphs of AP-1, AP-2, and AP-3 are shown in Fig. 4(A). The results indicate that the cP value of AP-1 was 27840–6930, AP-2 was 2332–165, and AP-3 was 900–78, while the spindle range was 0.5–4.00 rpm. When the spindle speed was set between 10 and 100 rpm, the cP value of AP-1 was recorded as 3027 to 633, but the cP values of AP-2 and AP-3 were undetectable owing to the low viscosity. The decrease in viscosity of polysaccharides typically depends on ultrasonic power, ultrasonic duration, temperature, pH, and the concentration of polysaccharide solution. High-intensity

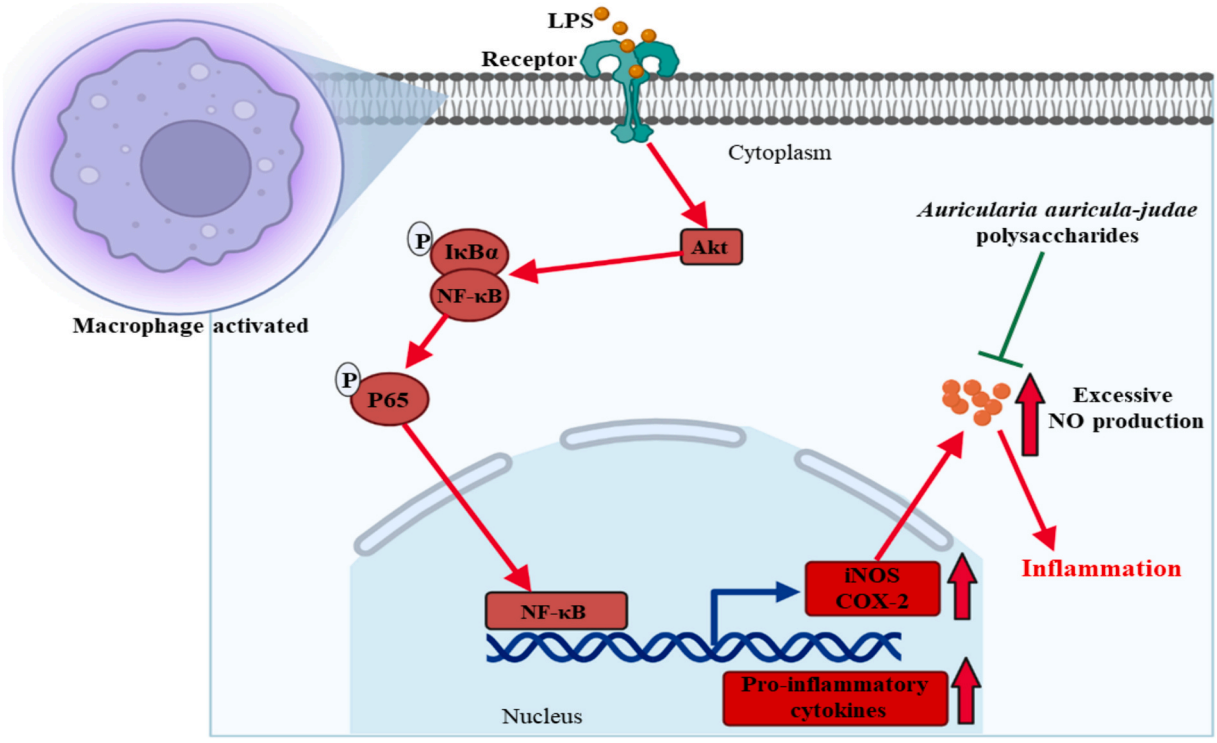

Fig. 3. Mechanisms of LPS on the progression of inflammation. Through the (TLRs) receptor, LPS activated macrophages and activated NF-κBs signaling, thereby increasing the production of pro-inflammatory cytokines as well as activated COX-2 and iNOS, while iNOS produces excessive levels of NO and leads to inflammation. On the other hand, *A. auricula-judae* polysaccharides inhibit NO production.

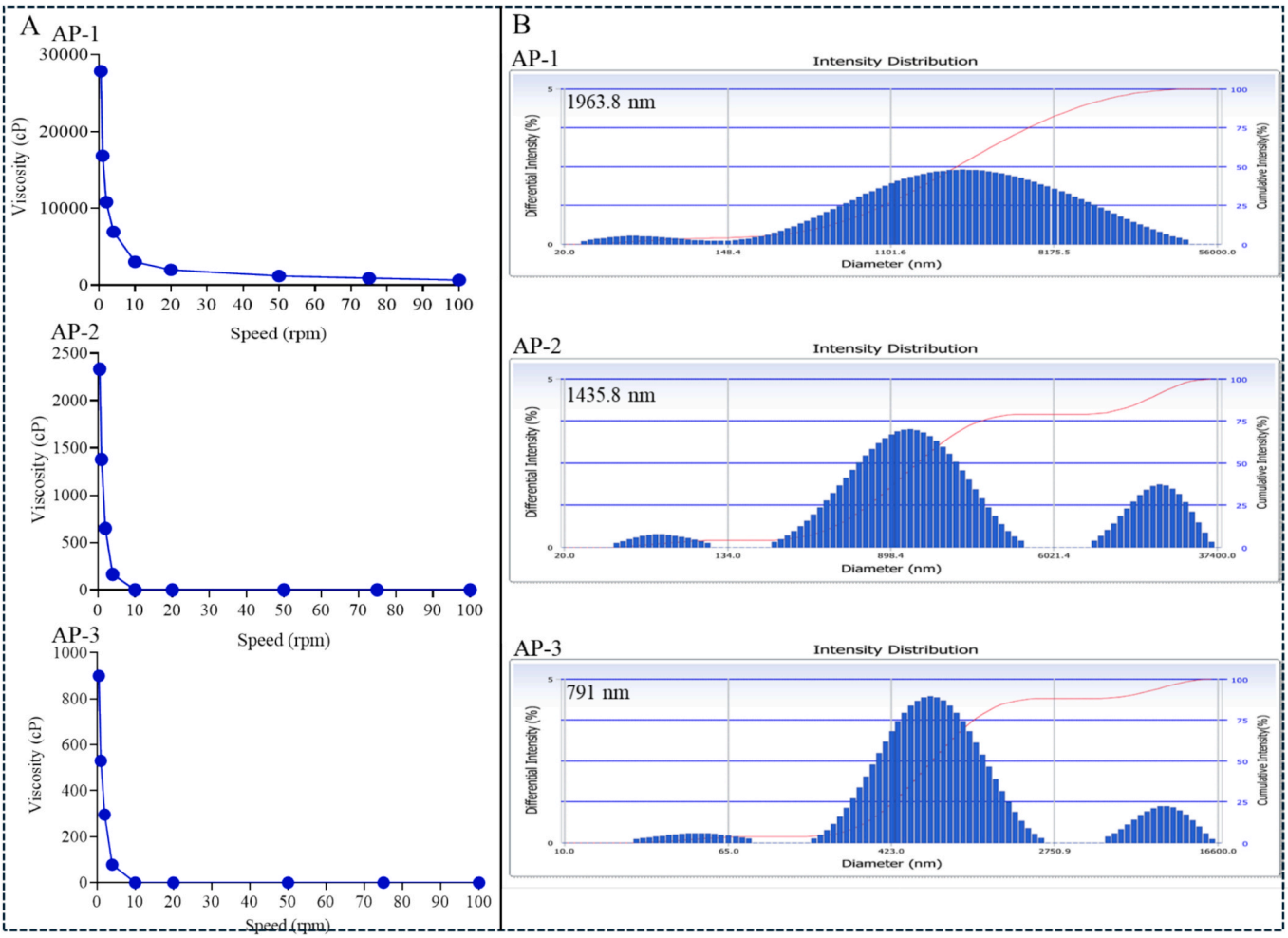

Fig. 4. The effects of ultrasonic degradation on *A. auricula-judae* polysaccharide's viscosity and particle size. (A) The initial viscosity of AP-1 was 27,840 cP; after ultrasonic degradation at different times, the initial viscosity values were 2332 cP in AP-2 and 900 cP in AP-3, recorded at 0.5 rpm speed. (B) The results show that the particle size was significantly reduced after ultrasonic degradation.

ultrasonication has been shown to affect chitosan's inherent viscosity, as previously described [6]. The current findings demonstrate that extending the duration of the ultrasonic process reduced the viscosity of *A. auricula-judae* polysaccharide. Due to their large molecular weight, low solubility, and higher viscosity, polysaccharides provide a significant challenge in functional food development and pharmaceutical areas. According to the literature, high molecular weight polysaccharides are known to have poor solubility and high viscosity, which showed a similar state to our current results [21]. Our current data suggest that ultrasonic treatment is one of the most effective methods for modifying polysaccharides' viscosity forms, which are more amenable to being dissolved in water.

The particle size distribution of native and degraded *A. auricula-judae* polysaccharides is presented in Fig. 4(B). The average particle size distribution of native polysaccharide (AP-1) was found at 1963.8 nm. However, after ultrasonic degradation, the average particle size distribution in AP-2 and AP-3 decreased to 1435.8 nm and 791 nm, respectively. Some research has shown that polysaccharides with a higher molecular weight also tend to have a large particle size, suggesting that particle size may be a surrogate for the molecular weight of polysaccharides [17,78]. The size of polysaccharide particles has a crucial impact on functional drug delivery [5]. Their particle size typically causes the low bioavailability of medications, inability to dissolve in water, and inability to pass through the cell membrane and epithelium [46]. By reducing the particle size of the polysaccharide, an external stimulus might initiate the release of the medication [15].

3.4. AFM, XRD, SEM, and EDX analysis of native and degraded *A. auricula-judae* polysaccharides

Polysaccharides have been examined extensively using atomic force microscopy (AFM) in recent years since AFM is an excellent method for characterizing biopolymers [1]. AFM was utilized to investigate the morphology and topography of AP-1, AP-2, and AP-3 polysaccharides of *A. auricula-judae* in aqua solution, providing direct evidence concerning the chain of conformation and macromolecular structure of these polysaccharides. Fig. 5(A) shows the AFM topographical images of AP-1, AP-2, and AP-3. These topographic images demonstrate linear, circular, and crossover patterns of AP-1, AP-2, and AP-3. The images demonstrate that AP-1 with a high molecular weight compacted folded into ribbon triple-helical chains, although most triple helix structures exist as modest intrachain entangled species. The structure of *A. auricula-judae* polysaccharide chains became chaotic, the branching chains became soft, short, and low polysaccharide chains, and even in AP-3, polysaccharide chains were linked to create single and random coils after treatment with ultrasound at different times. In AP-1, the ribbon and

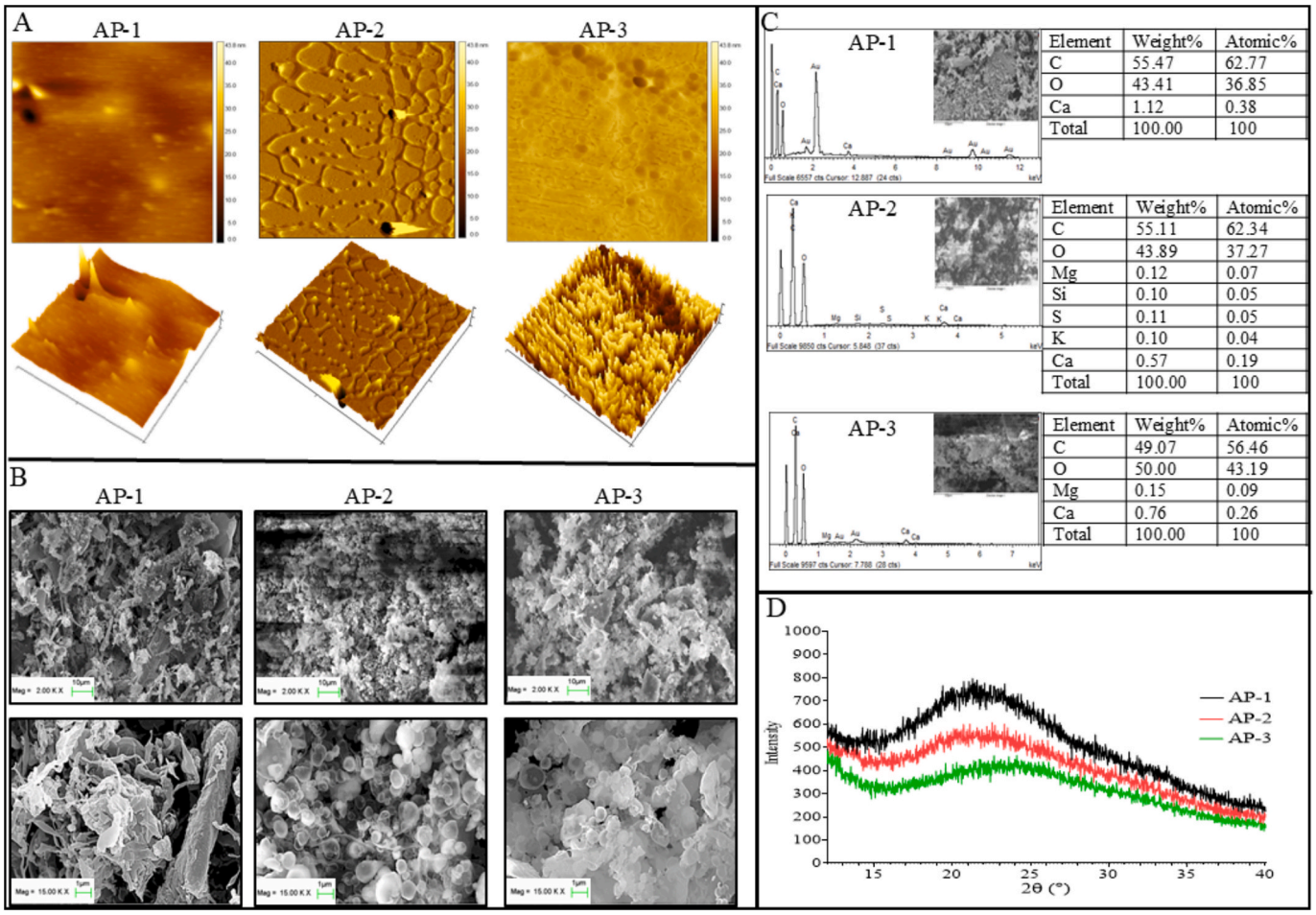

Fig. 5. Structural and elements analysis of native and degraded *A. auricula-judae* polysaccharides. (A) Topographical AFM planar and 3D images of native AP-1 (High MW) and degraded AP-2 (Medium MW) and AP-3 (Low MW) *A. auricula-judae* polysaccharides; (B) Scanning electron microscope (SEM) images of *A. auricula-judae* polysaccharides before and after ultrasonic degradation. AP-1 (High MW), AP-2 (Medium MW), and AP-3 (Low MW); (C) Energy dispersive x-ray spectroscopy (EDX) analysis for elements determination of native and degraded *A. auricula-judae* polysaccharides; (D) XRD (X-ray diffraction) intensity curves of native (AP-1) and ultrasonic degraded (AP-2 and AP-3) *A. auricula-judae* polysaccharides. Curves show that the ultrasonic degradation caused a reduction in the crystallinity of the polysaccharides.

triple helix structure began to transform into a single helix in AP-2, whereas, in AP-3, the random coil and single helix chains were more prominent than in AP-2. Consistent with earlier research, the polysaccharides with single-helix structures have higher anti-inflammatory activity [19].

Scanning electron microscopy (SEM) was used to examine the microstructure and topography of native and degraded *A. auricula-judae* polysaccharides. Fig. 5(B) represents the SEM images of AP-1, AP-2, and AP-3 polysaccharides with different molecular weights. AP-1 polysaccharide is shown to have altered into a spherical, irregular shape with massive particles, whereas AP-2 and AP-3 polysaccharides were seen to have altered into fine particle sizes. Before and after ultrasonic degradation, the microstructure of *A. auricula-judae* polysaccharide was intuitively evaluated using scanning electron microscopy (SEM). As shown the huge irregular particle size in native *A. auricula-judae* polysaccharide (AP-1), following ultrasonic degradation, the particle and structure were fragmented into smaller portions with a porous surface and cavities on the fracture surface, which may have been generated by the ultrasonic's considerable cavitation activity, turbulence shear, and instantaneous high pressure [12,13,39].

SEM-EDX was used to examine the chemical elements in native and degraded *A. auricula-judae* polysaccharides, detecting C, O, Mg, Si, S, K, and Ca. Fig. 5(C) depicts the various element peaks and the element and atomic percentage in AP-1, AP-2, and AP-3. In AP-1, chemical elements C (55.47 %), O (43.41 %), and Ca (1.12 %) were found; in AP-2, chemical elements C (55.11 %), O (43.89 %), Ca (0.57 %), Mg (0.12 %), Si (0.10 %), S (0.11 %), and K (0.10); and in AP-3, chemical elements C (49.07 %), O (50.00 %), Ca (0.76 %), and Mg (0.15 %). In these three different molecular weight polysaccharides from *A. auricula-judae*, C and O were identified as the main chemical elements. According to the elements analysis of AP-1, AP-2, and AP-3, the element's content in polysaccharides was evaluated, and the percentage of the principal elements was determined to be C and O. It has been noted that some polysaccharides include a small quantity of nitrogen; however, nitrogen was not detected in this *A. auricula-judae* polysaccharides. Rich samples of polysaccharides do not contain nitrogen, while they may include trace amounts of nitrogen derived from protein [66]. Trace amounts of minerals (Ca, Mg, S, and K) were detected in AP-1, AP-2, and AP-3 polysaccharides, which could be from the sources of polysaccharides or contamination from several factors, including extraction and

degradation process, the sensitivity of the analytical techniques, or the sample career contamination. Previous studies conducted EDX analysis with purified polysaccharides to investigate the contents of the major elements, whereas trace levels of minerals (Na, S, Ca, P, Cl) were detected, which have been ignored [42,48]. These findings indicated that this polysaccharide-rich sample of *A. auricula-judae* mushroom had a high concentration of polysaccharides, while C and O are the major elements.

The XRD profile of native and ultrasonic degraded *A. auricula-judae* polysaccharides is presented in Fig. 5(D). Results show that AP-1 had a higher intensity peak in 2θ range of 17-25° due to the crystalline aggregates, which are significantly related to the presence of an intermediate phase, hydrogen bonds, and triple-helical structure. However, the intensity of ultrasonic degraded AP-2 and AP-3 polysaccharides peaks was reduced, demonstrating the reduction in the polysaccharides' crystallinity and may alter the helical structure into a single helix. Previous studies have reported that lowering polysaccharides or cellulose crystallinity could alter the helical structure from triple helix to single helix, enhance digestibility, promote healthy gut microbiota, and increase anti-inflammatory effects [19,47,63].

3.5. Effects of native and degraded A. auricula-judae polysaccharides on body weight, DAI, behavior, colon lengths, and spleen weights in DSS-induced colitis mice

The anti-inflammatory effects of native (AP-1) and ultrasonic degraded (AP-2 and AP-3) *A. auricula-judae* polysaccharides were investigated in a DSS-induced colitis mouse model. It has been shown that the histological characteristics of mouse colitis produced by DSS are similar to those of human colitis [9]. Mice were subjected to three cycles of DSS water treatment to induce colitis, with the animals drinking DSS-free water during the recovery period (Fig. 6(A)). The common symptoms of inflammatory colitis, such as body weight changes, diarrhea, blood in stool, and colon length, were examined in the mice to confirm the successful induction of colitis by DSS. The DSS group mice showed significant reduction in body weight, increased DAI score, shorter colon length, and increased spleen weight (Fig. 6(B-F)); these findings were consistent with the earlier research [16]. After being treated with 5-ASA, AP-1, AP-2, and AP-3 at various dosages in mice with DSS-induced colitis, the body weights were increased, reduced the DAI score, spleen weight, and increased the colon length, whereas the AP-HD group had better recovery as compared to other treatment groups. Ulcerative colitis (UC) is an inflammatory and destructive disease of the large intestinal tract that often affects the rectum, the lower colon, and the whole colon [24]. Bodyweight changes, colon length, disease activity index (DAI), and spleen weight are commonly used to evaluate the severity of DSS-induced colitis, and it has been documented in several studies that DSS water intake in mice has a considerable impact on body weight loss and colon length reduction [16,76,88]. Our current result suggests that degraded *A. auricula-judae* AP-3 polysaccharide had better recovery effects from the above-mentioned inflammatory colitis symptoms.

3.6. Effects of native and degraded A. auricula-judae polysaccharides on colon histological changes and pro-inflammatory cytokines expression in DSS-induced colitis mice

H&E and alcian blue staining were performed on the colon tissue section to evaluate the anti-inflammatory effects of AP-1, AP-2, and AP-3 *A. auricula-judae* polysaccharides in DSS-induced colitis mice colon histological changes. Mice with recurrent DSS-induced chronic colitis displayed intestinal barrier degradation, decreased crypts, intensified inflammatory infiltration in the colon, and a rise in the histological score, while AP-1, AP-2, and AP-3 treatment exhibited reduced damages (Fig. 7(A,C)), whereas AP-3 HD had the most significant reduction in intestinal barrier degradation, inflammatory cell infiltration, and crypt destruction among the treatment groups. Colitis animal models have shown that DSS may damage colonic tissue, resulting in an increased histology score due to inflammation and crypt destruction that can be mitigated with proper medication [79,87]. In another study, colon tissue lesions were seen in the DSS group of mice, including crypt deformation, goblet cell loss, severe epithelial destruction, and mucosal infiltration of inflammatory cells [10]. In addition, it was postulated that AP-3 was much more effective in protecting intestinal mucosa from harm by enhancing its ability to heal itself. To further confirm this, alcian blue staining was conducted to examine the expression of intestinal mucin. Results show that the expressions of mucins, which were engaged in the healing of colon mucosa, were significantly lower in the DSS group compared to the control group (Fig. 7(B,D)). Despite this, high dosages of AP-1, AP-2, and AP-3 boosted mucin expressions, while AP-3 HD induced the most significant enhancement. Intestinal mucins are secreted by goblet cells that have a cytoprotective role against various hazards, including colonization by bacterial toxins [52]. Mucins are also responsible for protecting the underlying epithelium; a change in the amount of mucus secreted may affect the efficacy of this protective barrier and have serious physiological impacts [57,62]. These findings prove that AP-3 suppresses colonic inflammation and boosts mucosal repair.

It is well-established that inflammatory cytokines play a crucial role in the pathophysiology of colitis. To examine the anti-inflammatory effects of AP-1, AP-2, and AP-3, the secretion of pro-inflammatory cytokines TNF-α, IL-1β, and IL-6 was assessed using ELISA. The levels of these pro-inflammatory cytokines were much higher in the DSS group than in the control group (Fig. 7(E-H)). TNF-α in blood serum, TNF-α, IL-1β, and IL-6 in the colon were reduced following treatment with AP-1, AP-2, and AP-3 in comparison to the DSS group. Nevertheless, pro-inflammatory cytokine secretions were significantly reduced in the AP-3 HD group. The inflammatory response is considered to be a crucial mechanism in the pathophysiology of chronic colitis due to its role in regulating the immune system [31]. Macrophage migration and the production of inflammatory mediators may be triggered by pro-inflammatory cytokines, which play an active role in inflammatory progression[85]. Prior research has shown that recurrent DSS-induced chronic colitis is characterized by elevated levels of pro-inflammatory cytokines [32]. This study found that AP-1, AP-2, and AP-3 had potential anti-inflammatory effects through the inhibition of TNF-α, IL-1β, and IL-6 secretion, with AP-3 HD being the most effective.

3.7. Anti-inflammatory activity of AP-3 polysaccharide via suppressing iNOS, COX-2, NF-κBs, and enhancing tight junction proteins expression in the colon of DSS-induced colitis mice

The above results clarify that AP-3 has better anti-inflammatory effects in DSS-induced colitis mice. To further investigate the anti-inflammatory mechanism of AP-3 polysaccharide, the protein expression of tight junction (ZO-1), iNOS, COX-2, and NF-κBs (p65, p-p65, p-IκBα) were measured in colon tissue and the results are presented in Fig. 8. Zonula occludens-1 (ZO-1) is a tight junction protein that plays a vital role in maintaining the integrity of the intestinal mucosal barrier. To examine the ameliorative effects of AP-3 on intestinal barrier integrity, the expression of ZO-1 in colon tissue samples was analyzed using immunofluorescence. Fig. 8(A-B) shows the optical density of ZO-1 immunofluorescence-stained images of colon tissue. ZO-1 expression was considerably lower in the DSS group than in the control group. However, after being treated with AP-3, the mice showed a significant

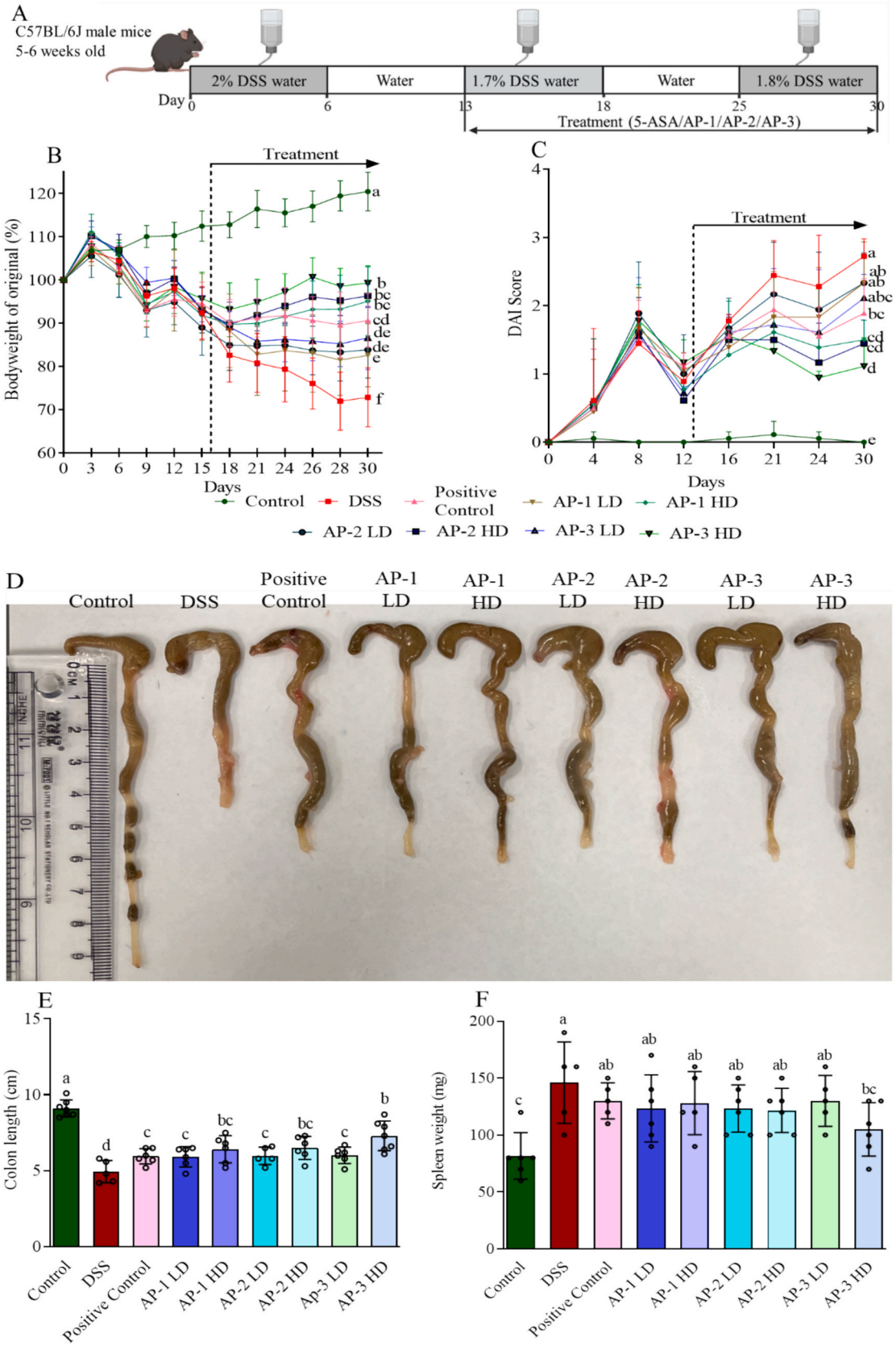

Fig. 6. Effects of AP-1, AP-2, and AP-3 *A. auricula-judae* polysaccharides on body weight changes, DAI score, spleen weight, and colon length in DSS-induced colitis mice. (A) The experimental timeline and treatment of DSS-induced colitis mice; (B) Bodyweight was recorded 2–3 times weekly (treatment from day 13 to day 30); (C) DAI scores were recorded at specific time points (treatment from day 13 to day 30); (D) DAI scores were collected according to the following parameters; (D) Representative image of the colon; (E) Measurement of colon length, and (F) Spleen weight. Data are expressed as mean ± SD. The parameters marked by the same letter are not significantly different, $p < 0.05$.

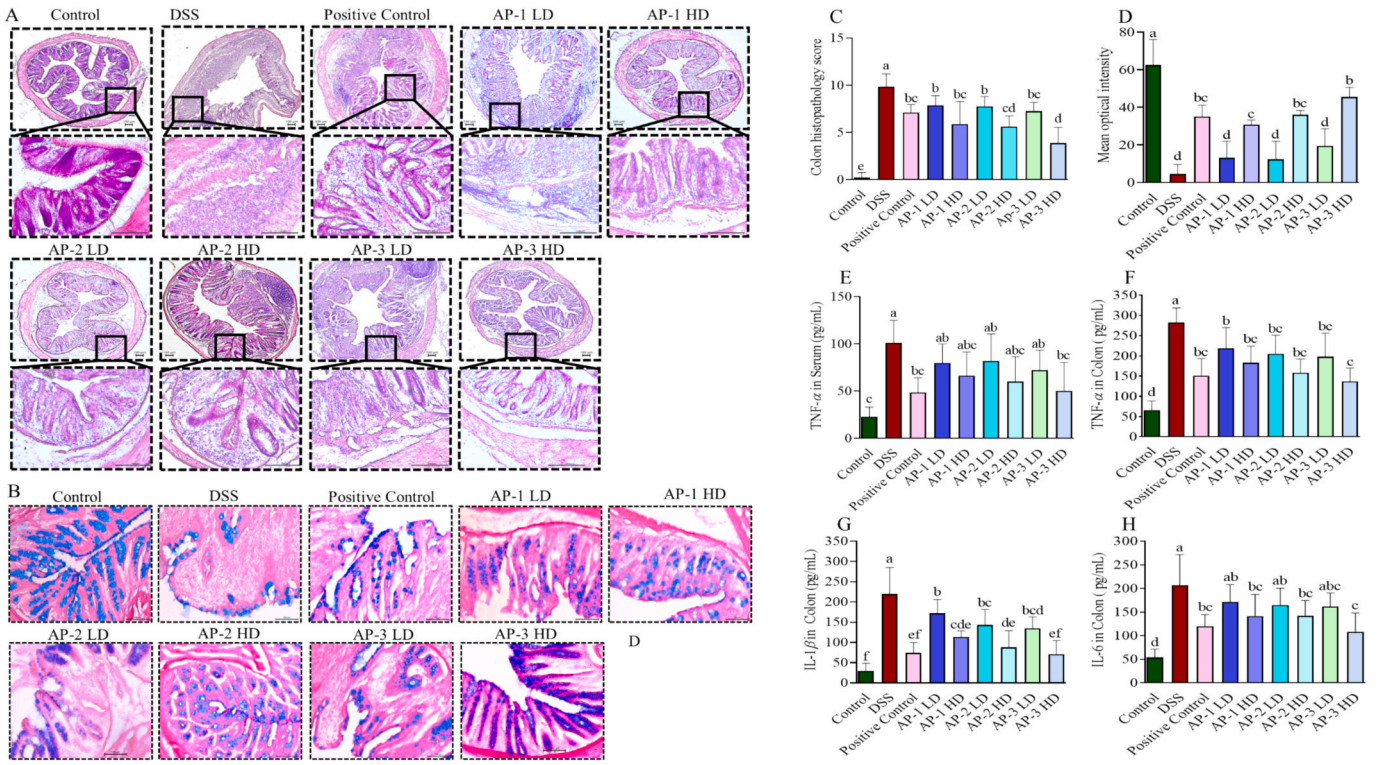

Fig. 7. Effects of native and degraded different MW *A. auricula-judae* polysaccharides on colon histopathological changes and pro-inflammatory cytokines expression in DSS-induced colitis mice. (A) Representative image of H&E staining of colon tissues, (B) representative image of alcian blue staining of mucin expression in colon tissue, (C) histological scores, (D) alcian blue optical density. Pro-inflammatory cytokines level of TNF-α in serum (E) and TNF-α (F), IL-1β (G), IL-6 (H) in the colon. Data are expressed as mean ± SD. Parameters marked by the same letter are not significantly different, $p < 0.05$.

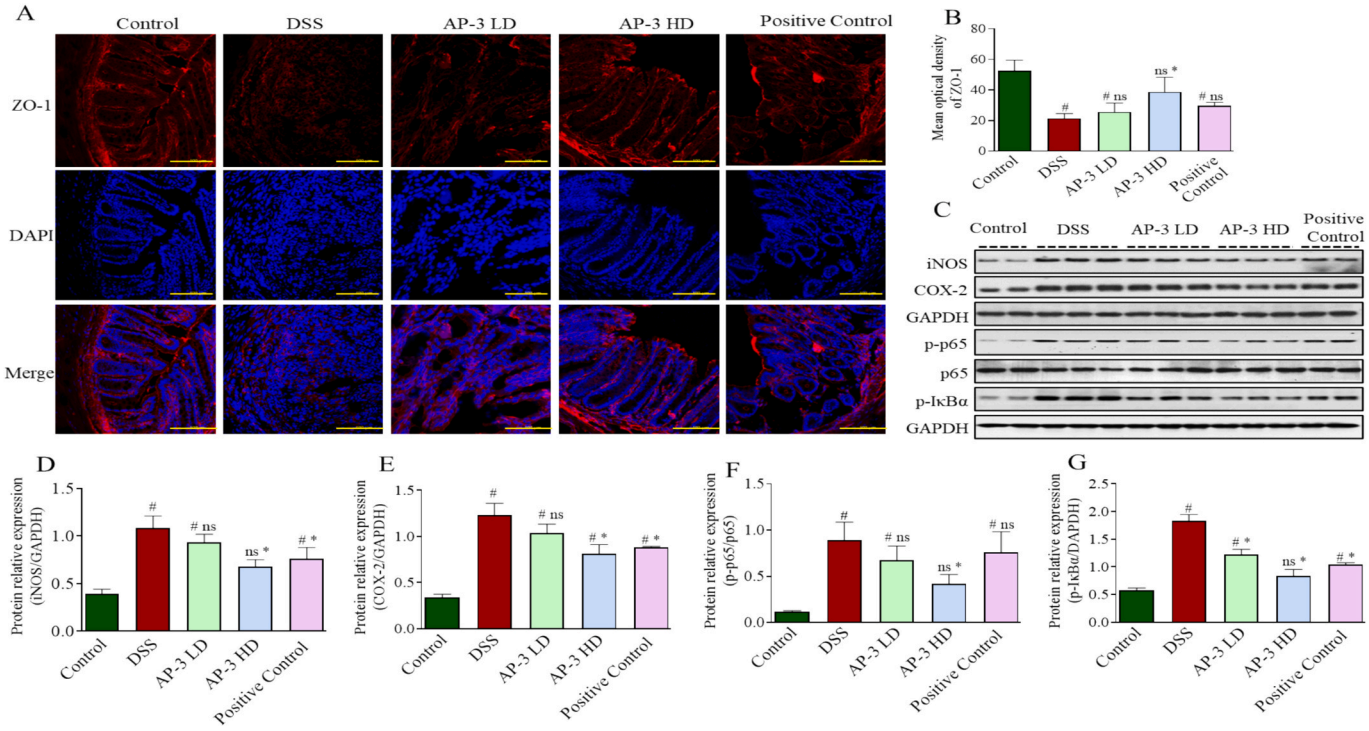

Fig. 8. AP-3 enhanced tight junction proteins and suppressed iNOS, COX-2, and NF-κB in the colon tissue of DSS-induced colitis mice. (A) Representative images of ZO-1 staining in colon tissues from different groups, (B) average optical density of ZO-1 staining across groups. (C) Representative images of immunoblot relative protein expression levels, (D-G) relative quantification of iNOS, COX-2, p-p65, and p-IκBα protein levels in colon tissues. Data are expressed as mean ± SD. # $p < 0.05$, compared with the control group; *$p < 0.05$, compared with the DSS group; ns, not significant.

improvement as compared to the DSS group, where ZO-1 expression dramatically increased in colon tissue. Intestinal epithelial cells use a protein cluster called the tight junction complex to create a physiologically active barrier whose permeability may be adjusted in response to local conditions [53]. It has been found that intestinal permeability was increased in animals with colitis produced by dextran sulfate sodium (DSS), and the expression of tight junction proteins in the ZO-1 was reduced [35,53]. Western blot results show that the DSS group significantly increased the expression of iNOS and COX-2 in the colon tissues of mice, while both protein expressions were significantly decreased in mice groups treated with AP-3 (Fig. 8(D-E)). The DSS group had considerably higher expression of NF-κB p65, p-p65, and p-IκBα as compared to the control group; alternatively, in the AP-3 treatment groups, p-p65 and p-IκBα expression were significantly lower than the DSS group (Fig. 8(F-G)). NF-κB is a major modulator of immune cell responses to inflammation, DNA damage, oxidative stress, genotoxic damage, and dysregulated NF-κB signaling causes inflammation in multiple diseases such as multiple sclerosis, rheumatoid arthritis, and various inflammatory bowel diseases [58]. NF-κB activation enhances the transcription of genes involved in inflammatory responses, including iNOS, COX-2, IL-6, IL-1β, and TNF-α [4]. These results have shown a significant correlation with pro-inflammatory cytokine expression changes, which demonstrate AP-3′s possible protective benefits against colitis. Based on the current findings, the mechanisms of AP-3 polysaccharide in DSS-induced colitis mice are illustrated in Fig. 9.

3.8. Effects of AP-3 polysaccharide on gut microbiota structure in DSS-induced colitis mice

To explore the anti-inflammatory effects of AP-3 polysaccharide in DSS-induced mice, 16S rRNA gut microbial sequencing was further performed on mice fecal samples. Three groups of mouse feces samples were selected and renamed for investigation of gut microbiota: Control, DSS, and AP-3 HD group. The abundance index (Chao and ACE) and diversity index were used to determine the alpha diversity index (Shannon and Simpson). There was a statistically significant difference between the DSS and control groups, as well as between the DSS and AP-3 HD groups, as measured by the alpha diversity index of the fecal microbiota (Fig. S1). According to the data, the DSS group had a lower alpha diversity index than the control group. However, compared with the DSS group, the alpha diversity index was raised in AP-1 HD group.

The top 10 gut microbiota at the phylum level and top 20 gut microbiota at the genus level are shown in Fig. 10. The different mouse phyla in each group are shown in Fig. 10(A), whereas the different groups' phylum distributions are shown in Fig. 10(B). The most abundant phylum were determined to be *Firmicutes, Bacteroidetes, Proteobacteria, Tenerobacteria, Actinobacteria,* and *Deferribacteres,* within the order. Meanwhile, the *Bacteroidetes* phylum was more prevalent in the Control and AP-3 HD than in the DSS. Furthermore, the individual relative abundance percentage of *Proteobacteria, Firmicutes* at the phylum level, and G*ammaproteobacteria* at the class level were higher in the DSS as compared to control and AP-3 HD groups, while *Bacteroidetes* at the phylum level was lower in DSS as compared to Control and AP-3 HD (Fig. 11(A-D)). Fig. 11(E-I) demonstrates that the relative abundance of *Allobaculum*, *Alloprevotella*, and *Prevotella* at genus level was lower in the DSS group, while those were highest in the Control and AP-3 HD groups, while *Romboutsia* and *Escherichia-Shigella* were more prevalent in the DSS group.

Furthermore, spearmen correlation analysis revealed that the unhealthy gut microbiota *Romboutsia* and *Escherichia-Shigella* exhibited a negative correlation with body weight changes, colon length, and mucin expression (alcian blue) in the colon. Conversely, these genera showed a positive correlation with H&E staining, TNF-α, IL-1β, and IL-6 levels. In contrast, the healthy gut microbiota *Allobaculum*, *Prevotella*, and *Alloprevotella* were positively correlated with bodyweight changes, colon length, and mucin expression (alcian blue) in the colon, while showing a negative correlation with H&E staining, TNF-α, IL-1β, and IL-6 levels (Fig. S3). These findings suggest that the degradation of polysaccharides significantly influences gut microbiota composition, contributing to the prevention of colitis.

Further LEfSe analysis was performed to identify the biomarker species with significant changes between the control and DSS groups, and the DSS and AP-3 HD groups. LDA (Linear Discriminant Analysis) was used to minimize the dimension and analyze the effect of the various species. The rank-sum test was performed to identify the different species among the different groups. Histogram of LDA values, phylogenetic tree map (phylogenetic distribution), and biomarker abundance comparison tree map showing statistically significant differences between

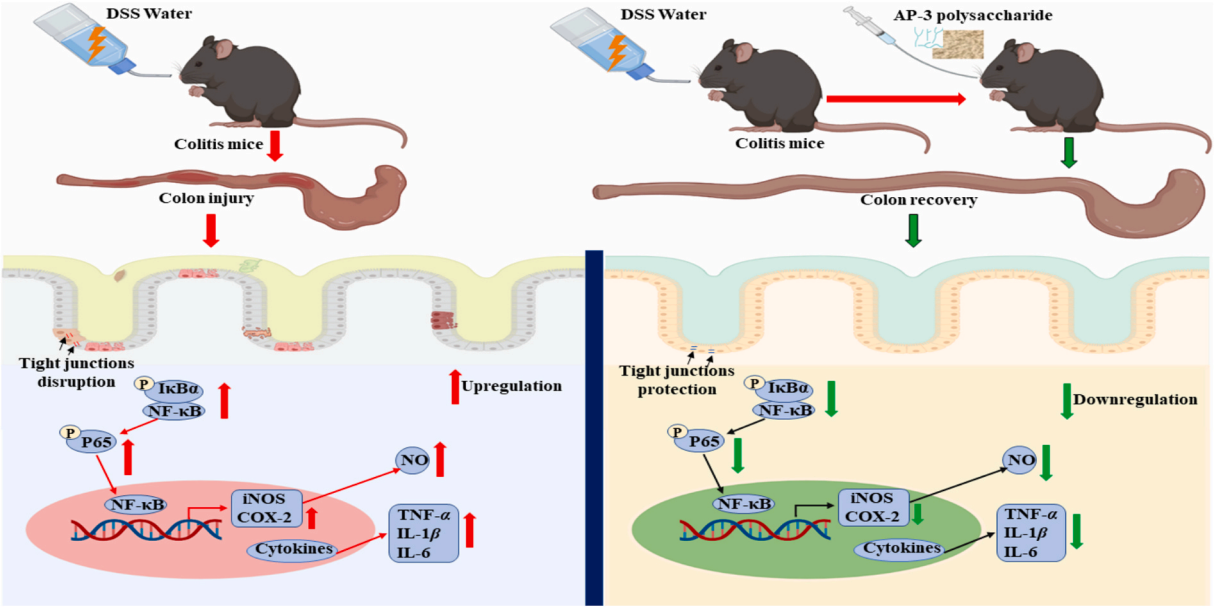

Fig. 9. The DSS-induced colitis mice showed intestine epithelium cells were damaged, mucin and tight junction proteins were disrupted, and activated NF-κBs signaling, thereby enhancing iNOS, COX-2, and pro-inflammatory cytokines significantly. After being treated with AP-3 polysaccharide to colitis mice, iNOS, COX-2, pro-inflammatory cytokines, and NF-κBs proteins expression were suppressed, while tight junction proteins of ZO-1 and mucin were enhanced significantly.

Fig. 10. The gut microbial composition at the phylum and genus levels in different mice and groups. (A) Each column represents the percentage of relative abundance of bacterial phylum for each mouse, (B) each column represents the percentage of relative abundance of bacterial phylum level of each group, and (C) each column represents the percentage of relative abundance of bacterial genus for each mouse.

groups. *Enterobacteriaceae, Bacilli, Proteobacteria,* and *Gammaproteobacteria* were discovered to have LDA values more than 4.0 in the DSS, while these bacteria were not detected in the control group (Fig. S2(A)). The majority of *Bacteroidetes*, *Prevotellaceae*, and *Allobaculum* had LDA scores of more than 4 in the control group, while in AP-3 HD group, the majority of *Prevotellaceae*, *Prevotella*, and *Allobaculum* had over 4 LDA scores. *Gammaproteobacteria, Enterobacteriales*, and *Escherichia-Shigella* showed higher LDA scores in the DSS group, while these bacteria were not found in the AP-3 HD group (Fig. S2(B)).

Dysbiosis of the gut microbiome plays a critical role in activating the immune system, and numerous studies have shown that gut microbial dysbiosis is directly associated with the course of UC, and those have been documented in our review [28]. We investigated the effect of degraded low molecular weight (AP-3) *A. auricula-judae* polysaccharide on the intestinal microbiota of mice with DSS-induced colitis. Results show that the alpha diversity improved in the AP-3 HD compared to the DSS group. The LDA score and relative abundance of *Gammaproteobacteria*, *Enterobacteriaceae, and Escherichia-Shigella* were considerably greater in the DSS group but were not found in the Control or AP-3 HD groups. It has been shown that *Gammaproteobacteria* and *Enterobacteriaceae* have the ability to induce aberrant activation of the immune system [72]. Another research indicated that the quantity of *Enterobacteriaceae* and *Gammaproteobacteria* was strongly connected with the release of inflammatory cytokines, which was consistent with the findings of the present investigation [23]. In a recent study, it was reported that the genus *Romboutsia* is considered a pro-inflammatory gut microbiota, which can contribute to colitis and found a relatively higher abundance of *Romboutsia* in DSS-induced colitis mice, which aligns with our current findings [16]. In contrast, the abundance of *Allobaculum* and *Alloprevotella* was comparatively more significant in the Control and AP-3 HD groups, whereas it was considerably lower in the DSS group. *Allobaculum* provides a protective function in moulding the adult

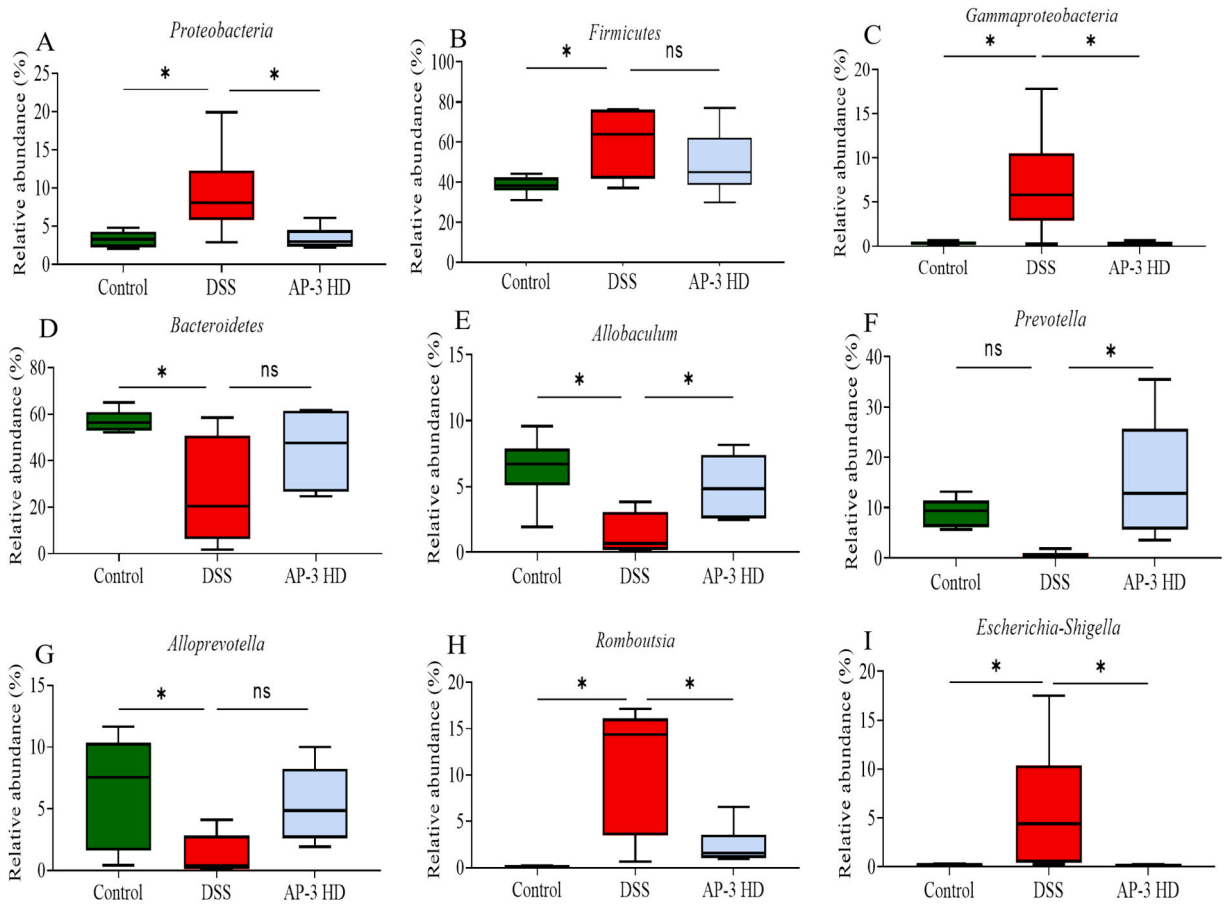

Fig. 11. The percentage of relative abundance at the phylum, class, and genus levels in different groups. (A) *Proteobacteria*(p), (B) *Firmicutes*(p), (C) *Gammaproteobacteria*(c), (D) *Bacteroidetes*(p) (E) *Allobaculum*(g), (F) *Prevotella*(g), (G), *Alloprevotella*(g), (H) *Romboutsia*(g), and (I) *Escherichia-Shigella* (g). * $p < 0.05$ compared with the corresponding group.

metabolism and in anti-inflammatory activity [54,69]. Growing more of the *Allobaculum* genus might protect mice from developing UC since this significant genus is inversely related to the disease [51]. The bacteria *Alloprevotella* has been shown to have anti-inflammatory and gut-barrier-supporting properties by producing succinate and acetate [18]. The molecular weight of polysaccharides plays a critical role in the structure of gut microbiota. Generally, high molecular weight polysaccharides cannot be fully degraded and fermented by the gut microbiota, while the gut microbiota efficiently utilizes low molecular weight polysaccharides [74]. Therefore, based on our current results, we can conclude that AP-3 ultrasonic degraded low molecular weight *A. auricula-judae* polysaccharide has a higher ability to improve intestinal gut microbial diversity by increasing healthy microbes and protecting unhealthy ones. Healthy gut microbiota has significant effects on repairing leaky gut via SCFA production. Compared with preliminary experimental gut microbiota data, this current finding reveals that degraded low molecular weight *A. auricula-judae* polysaccharide had higher effects in regulating healthy gut microbiota and protecting them from unhealthy gut microbiota, as this polysaccharide metabolized and utilized more efficiently by gut microbiota than the native polysaccharide. The gut microbiota regulating mechanisms of different molecular weight polysaccharides are illustrated in Fig. 12.

4. Conclusion

In conclusion, the ultrasonic degradation of *A. auricula-judae* polysaccharides yielded promising results as a potent anti-inflammatory agent. The polysaccharide's molecular weight, viscosity, particle size, and helical structure were significantly associated with its anti-inflammatory activity, and these properties were effectively modulated through ultrasonic degradation. The resulting change in helical structure, from a ribbon and triple structure into a single helix and random coil structure, appears to be closely related to its enhanced anti-inflammatory activity. When applied to the DSS-induced colitis mouse model, AP-3 showed the most remarkable therapeutic effects by reducing inflammatory symptoms, decreasing pro-inflammatory cytokine secretion, downregulated NOS, COX-2, and NF-κB signaling-related protein expression levels, and notably increasing ZO-1 protein in the colon. Additionally, the 16S rRNA gut microbiota analysis indicated that AP-3 treatment led to a meaningful shift in the gut microflora, suppressing unhealthy microbiota such as *Gammaproteobacteria*, *Enterobacteriaceae*, *Firmicutes*, and *Escherichia-Shigella* while promoting the growth of beneficial gut microbiota such as *Allobaculum, Alloprevotella*, and *Bacteroidetes*. Therefore, the polysaccharide derived from *A. auricula-judae*, particularly in its ultrasonically degraded form (AP-3), demonstrated significant anti-inflammatory properties. In conjunction with the abundance of bioactive compounds in mushrooms, this finding suggests a promising potential for this polysaccharide in therapeutic applications and functional food product development. However, further extensive research into its molecular mechanism and clinical trials are needed to ascertain its potential as a potent anti-inflammatory therapeutic agent.

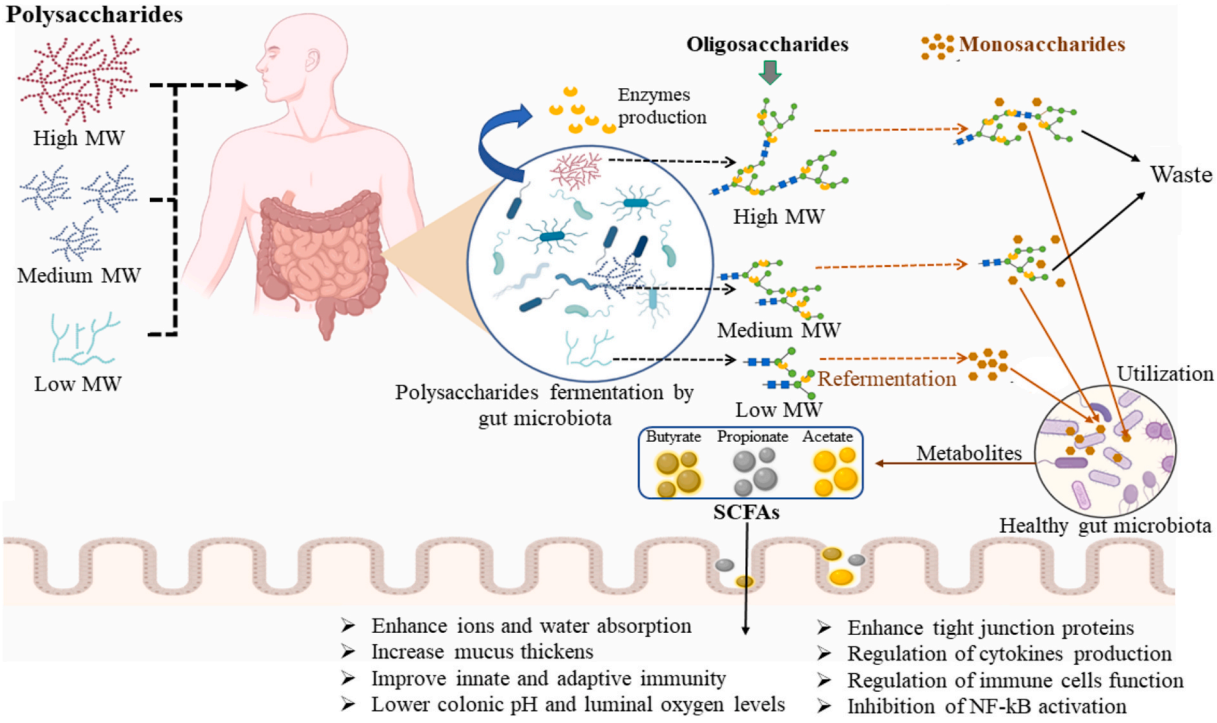

Fig. 12. Intestinal gut microbiota cannot completely ferment/degrade high molecular weight (MW) polysaccharides within 2–6 h; hence, the unfermented residual polysaccharides are flushed out from our bodies as waste. Low MW polysaccharides are readily fermentable and metabolizable by gut bacteria, enhancing gut health and protecting against various disorders.

Author Contributions

Tahidul Islam- Investigation and writing of the original draft. Boojum Xu: Supervision, writing-review and editing. Zhaoxiang Bian: Conceptualization, supervision, writing-review and editing, funding acquisition.

CRediT authorship contribution statement

Tahidul Islam: Writing – original draft, Visualization, Validation, Software, Methodology, Investigation, Formal analysis, Data curation. **Baojun Xu:** Writing – review & editing, Visualization, Validation, Supervision, Resources, Project administration, Methodology, Investigation, Funding acquisition, Conceptualization. **Zhaoxiang Bian:** Writing – review & editing, Validation, Supervision, Resources, Project administration, Methodology, Funding acquisition.

Funding

This research was supported by the National- Natural Science-Foundation of China (82000504 and 81973538), the Health and Medical Research Fund (17182661), the Health@InnoHK Initiative Fund of the Hong Kong Special Administrative Region Government (ITC RC/IHK/4/7), and in part by Guangdong Higher Education Upgrading Plan (2021–2025) with project code (UICR0400015-24 and UICR0400016-24), China.

Declaration of competing interest

The authors declare that they have no known competing financial interests or personal relationships that could have appeared to influence the work reported in this paper.

Appendix A. Supplementary data

Supplementary data to this article can be found online at https://doi.org/10.1016/j.ultsonch.2025.107339.

References

[1] N.I. Abu-Lail, T.A. Camesano, Polysaccharide properties probed with atomic force microscopy, J. Microsc. 212 (3) (2003) 217–238, https://doi.org/10.1111/j.1365-2818.2003.01261.x.
[2] M.R. Akanda, I.S. Kim, D. Ahn, H.J. Tae, H.H. Nam, B.K. Choo, K. Kim, B.Y. Park, Anti-inflammatory and gastroprotective roles of rabdosia inflexa through downregulation of pro-inflammatory cytokines and MAPK/NF-κB signaling pathways, Int. J. Mol. Sci. 19 (2) (2018), https://doi.org/10.3390/ijms19020584.
[3] S. Alban, G. Franz, Characterization of the Anticoagulant Actions of a Semisynthetic Curdlan Sulfate. In, Thromb. Res. 99 (2000).
[4] P.A. Baeuerle, V.R. Baichwal, NF-κB as a frequent target for immunosuppressive and anti-inflammatory molecules, Adv. Immunol. 65 (1997) 111–137. https://www.scopus.com/inward/record.uri?eid=2-s2.0-0030747128&partnerID=40&md5=41651daae4a2cf2094dca1d521dd0a5a.
[5] T.G. Barclay, C.M. Day, N. Petrovsky, S. Garg, Review of polysaccharide particle-based functional drug delivery, Carbohydr. Polym. 221 (2019) 94–112, https://doi.org/10.1016/J.CARBPOL.2019.05.067.
[6] S. Baxter, S. Zivanovic, J. Weiss, Molecular weight and degree of acetylation of high-intensity ultrasonicated chitosan, Food Hydrocoll. 19 (5) (2005) 821–830, https://doi.org/10.1016/j.foodhyd.2004.11.002.
[7] D. Buapool, N. Mongkol, J. Chantimal, S. Roytrakul, E. Srisook, K. Srisook, Molecular mechanism of anti-inflammatory activity of Pluchea indica leaves in macrophages RAW 264.7 and its action in animal models ofinflammation, J. Ethnopharmacol. 146 (2) (2013) 495–504, https://doi.org/10.1016/J.JEP.2013.01.014.
[8] J.G. Caporaso, J. Kuczynski, J. Stombaugh, K. Bittinger, F.D. Bushman, E. K. Costello, N. Fierer, A.G. Peña, J.K. Goodrich, J.I. Gordon, G.A. Huttley, S. T. Kelley, D. Knights, J.E. Koenig, R.E. Ley, C.A. Lozupone, D. McDonald, B. D. Muegge, M. Pirrung, R. Knight, QIIME allows analysis of high-throughput community sequencing data, Nat. Methods 7 (5) (2010) 335–336, https://doi.org/10.1038/nmeth.f.303.
[9] Chassaing, B., Aitken, J. D., Malleshappa, M., & Vijay-Kumar, M. (2014). Dextran sulfate sodium (DSS)-induced colitis in mice. Current Protocols in Immunology, SUPPL.104. https://doi.org/10.1002/0471142735.im1525s104.
[10] G. Chen, Y. Yang, M. Liu, Z. Teng, J. Ye, Y. Xu, X. Cai, X. Cheng, J. Yang, C. Hu, M. Wang, P. Cao, Banxia xiexin decoction protects against dextran sulfate sodium-induced chronic ulcerative colitis in mice, J. Ethnopharmacol. 166 (2015) 149–156, https://doi.org/10.1016/j.jep.2015.03.027.

[11] H. Chen, J. Yin, C. Yeh, Y. Lu, J. Yang, Inverse synthetic aperture radar imaging based on time–frequency analysis through neural network, J. Electron. Imaging 29 (01) (2020) 1, https://doi.org/10.1117/1.JEI.29.1.013003.
[12] J. Chen, R.-H. Liang, W. Liu, C.-M. Liu, T. Li, Z.-C. Tu, J. Wan, Degradation of high-methoxyl pectin by dynamic high pressure microfluidization and its mechanism, Food Hydrocoll. 28 (1) (2012) 121–129, https://doi.org/10.1016/j.foodhyd.2011.12.018.
[13] L. Chen, A. Abulizi, M. Li, Protective effect of Ganoderma (Lingzhi) on radiation and chemotherapy, Adv. Exp. Med. Biol. 1182 (2019) 119–142, https://doi.org/10.1007/978-981-32-9421-9_4/COVER.
[14] Y. Chi, M. Zhang, X. Wang, X. Fu, H. Guan, P. Wang, Ulvan lyase assisted structural characterization of ulvan from Ulva pertusa and its antiviral activity against vesicular stomatitis virus, Int. J. Biol. Macromol. 157 (2020) 75–82, https://doi.org/10.1016/J.IJBIOMAC.2020.04.187.
[15] T.A. Debele, S.L. Mekuria, S.-Y. Lin, H.-C. Tsai, Synthesis and characterization of bioreducible heparin-polyethyleneimine nanogels: application as imaging-guided photosensitizer delivery vehicle in photodynamic therapy, RSC Adv. 6 (18) (2016) 14692–14704, https://doi.org/10.1039/C5RA25650J.
[16] L. Deng, H. Guo, S. Wang, X. Liu, Y. Lin, R. Zhang, W. Tan, The attenuation of chronic ulcerative colitis by (R)-salbutamol in repeated DSS-induced mice, Oxid. Med. Cell. Longev. 2022 (2022), https://doi.org/10.1155/2022/9318721.
[17] Z. Dou, C. Chen, X. Fu, The effect of ultrasound irradiation on the physicochemical properties and α-glucosidase inhibitory effect of blackberry fruit polysaccharide, Food Hydrocoll. 96 (2019) 568–576, https://doi.org/10.1016/j.foodhyd.2019.06.002.
[18] Downes, J., Dewhirst, F. E., Tanner, A. C. R., & Wade, W. G. (2013). Description of Alloprevotella rava gen. nov., sp. nov., isolated from the human oral cavity, and reclassification of Prevotella tannerae Moore et al. 1994 as Alloprevotella tannerae gen. nov., comb. nov. International Journal of Systematic and Evolutionary Microbiology, 63(PART4), 1214–1218. https://doi.org/10.1099/ijs.0.041376-0.
[19] B. Du, Effect of molecular weight and structure on anti-inflammatory properties of polysaccharide from submerged mycelial fermentation of schizophyllum commune, Hong Kong Baptist University, 2016.
[20] B. Du, Y. Yang, Z. Bian, B. Xu, Molecular weight and helix conformation determine intestinal anti-inflammatory effects of exopolysaccharide from Schizophyllum commune, Carbohydr. Polym. 172 (2017) 68–77.
[21] I.P.S. Fernando, D. Kim, J.-W. Nah, Y.-J. Jeon, Advances in functionalizing fucoidans and alginates (bio)polymers by structural modifications: A review, Chem. Eng. J. 355 (2019) 33–48, https://doi.org/10.1016/j.cej.2018.08.115.
[22] A.H. Fischer, K.A. Jacobson, J. Rose, R. Zeller, Cryosectioning tissues, Cold Spring Harb Protoc 3 (8) (2008), https://doi.org/10.1101/pdb.prot4991.
[23] Z. Gu, Y. Zhu, S. Jiang, G. Xia, C. Li, X. Zhang, J. Zhang, X. Shen, Tilapia head glycolipids reduce inflammation by regulating the gut microbiota in dextran sulphate sodium-induced colitis mice, Food Funct. 11 (4) (2020) 3245–3255, https://doi.org/10.1039/d0fo00116c.
[24] Guo, X., Luo, J., Qi, J., Zhao, X., An, P., Luo, Y., & Wang, G. (2022). The role and mechanism of polysaccharides in anti-aging. Nutrients 2022, Vol. 14, Page 5330, 14(24), 5330. https://doi.org/10.3390/NU14245330.
[25] X. Guo, X. Ye, Y. Sun, D. Wu, N. Wu, Y. Hu, S. Chen, Ultrasound effects on the degradation kinetics, structure, and antioxidant activity of sea cucumber fucoidan, J. Agric. Food Chem. 62 (5) (2014) 1088–1095, https://doi.org/10.1021/jf404717y.
[26] T. Hong, J.-Y. Yin, S.-P. Nie, M.-Y. Xie, Applications of infrared spectroscopy in polysaccharide structural analysis: Progress, challenge and perspective, Food Chem.: X 12 (2021) 100168, https://doi.org/10.1016/j.fochx.2021.100168.
[27] T. Islam, K. Ganesan, B. Xu, New insight into mycochemical profiles and antioxidant potential of edible and medicinal mushrooms: A review, International Journal of Medicinal Mushrooms 21 (3) (2019) 237–251, https://doi.org/10.1615/IntJMedMushrooms.2019030079.
[28] T. Islam, K. Ganesan, B. Xu, Insights into health-promoting effects of Jew's ear (Auricularia auricula-judae), Trends Food Sci. Technol. 114 (2021) 552–569, https://doi.org/10.1016/j.tifs.2021.06.017.
[29] Ji L, Jie Z, Ying X, Y. Q., & Zhou Y, S. L. (2018). Structural characterization of alkali-soluble polysaccharides from Panax. Royal Society Open Science, 5(3), 171644.
[30] I.H. Jung, D.E. Lee, J.H. Yun, A.R. Cho, C.S. Kim, Y.J. You, S.J. Kim, S.H. Choi, Anti-inflammatory effect of (-)-epigallocatechin-3-gallate on porphyromonas gingivalis lipopolysaccharide-stimulated fibroblasts and stem cells derived from human periodontal ligament, Journal of Periodontal and Implant Science 42 (6) (2012) 185–195, https://doi.org/10.5051/jpis.2012.42.6.185.
[31] Kai Wang, Xiaolu Jin, Li, Q., Alexandra Christine Helena Frankland, & K, R. (2018). Propolis from different geographic origins decreases intestinal inflammation and Bacteroides spp. populations in a model of DSS-induced colitis. Molecular Nutrition and Food Research, 62(7).
[32] Kanwal, S., Joseph, T. P., Aliya, S., Song, S., Saleem, M. Z., Nisar, M. A., Wang, Y., Meyiah, A., Ma, Y., & Xin, Y. (2020). Attenuation of DSS induced colitis by Dictyophora indusiata polysaccharide (DIP) via modulation of gut microbiota and inflammatory related signaling pathways. Journal of Functional Foods, 64(October 2019), 103641. https://doi.org/10.1016/j.jff.2019.103641.
[33] T.D. Kellock, S. Julie, M. Jurenka, Inflammatory bowel disease part i: ulcerative colitis – pathophysiology and conventional and alternative treatment options, Altern. Med. Rev. 4 (3) (2003) 247–283, https://doi.org/10.3109/09637485809142520.
[34] G. Kolios, V. Valatas, S.G. Ward, Nitric oxide in inflammatory bowel disease: a universal messenger in an unsolved puzzle, Immunology 113 (4) (2004) 427, https://doi.org/10.1111/J.1365-2567.2004.01984.X.
[35] W.-T. Kuo, L. Zuo, M.A. Odenwald, S. Madha, G. Singh, C.B. Gurniak, C. Abraham, J.R. Turner, The tight junction protein ZO-1 is dispensable for barrier function but critical for effective mucosal repair, Gastroenterology 161 (6) (2021) 1924–1939, https://doi.org/10.1053/j.gastro.2021.08.047.
[36] S.Y. Lee, H.J. Kim, J.S. Han, Anti-inflammatory effect of oyster shell extract in LPS-stimulated RAW 264.7 cells. Preventive, Nutr. Food Sci. 18 (1) (2013) 23, https://doi.org/10.3746/PNF.2013.18.1.023.
[37] G.B. Lenon, C.G. Li, C.C. Xue, F.C.K. Thien, D.F. Story, Inhibition of inducible nitric oxide production and iNOS protein expression in lipopolysaccharide-stimulated rat aorta and Raw 264.7 macrophages by ethanol extract of a Chinese herbal medicine formula (RCM-101) for allergic rhinitis, J. Ethnopharmacol. 116 (3) (2008) 547–553, https://doi.org/10.1016/J.JEP.2008.01.005.
[38] J. Li, C. Cai, M. Zheng, J. Hao, Y. Wang, M. Hu, L. Fan, G. Yu, Alkaline extraction, structural characterization, and bioactivities of (1→6)-β-d-glucan from lentinus edodes, Molecules 24 (8) (2019), https://doi.org/10.3390/molecules24081610.
[39] J. Li, S. Li, L. Wu, H. Yang, C. Wei, T. Ding, S. Chen, Ultrasound- assisted fast preparation of low molecular weight fucosylated chondroitin sulfate with antitumor activity, Carbohydr. Polym. 209 (2019) 82–91.
[40] M. Li, L. Dong, H. Du, Z. Bao, S. Lin, Potential mechanisms underlying the protective effects of Tricholoma matsutake singer peptides against LPS-induced inflammation in RAW264.7 macrophages, Food Chem. 353 (2021) 129452, https://doi.org/10.1016/j.foodchem.2021.129452.
[41] S. Li, Q. Xiong, X. Lai, X. Li, M. Wan, J. Zhang, Y. Yan, M. Cao, L. Lu, J. Guan, D. Zhang, Y. Lin, Molecular modification of polysaccharides and resulting bioactivities, Compr. Rev. Food Sci. Food Saf. 15 (2) (2016) 237–250, https://doi.org/10.1111/1541-4337.12161.
[42] Q. Liu, R. Ma, S. Li, Y. Fei, J. Lei, R. Li, Y. Pan, S. Liu, L. Wang, Dietary supplementation of Auricularia auricula-judae polysaccharides alleviate nutritional obesity in mice via regulating inflammatory response and lipid metabolism, Foods 11 (7) (2022), https://doi.org/10.3390/foods11070942.
[43] S. Liu, S. Zhang, X. Lv, J. Lu, C. Ren, Z. Zeng, L. Zheng, X. Zhou, H. Fu, D. Zhou, Y. Chen, Limonin ameliorates ulcerative colitis by regulating STAT3/miR-214 signaling pathway, Int. Immunopharmacol. 75 (2019) 105768, https://doi.org/10.1016/J.INTIMP.2019.105768.
[44] Y. Liu, Y. Zhou, M. Liu, Q. Wang, Y. Li, Extraction optimization, characterization, antioxidant and immunomodulatory activities of a novel polysaccharide from the wild mushroom Paxillus involutus, Int. J. Biol. Macromol. 112 (2018) 326–332, https://doi.org/10.1016/J.IJBIOMAC.2018.01.132.
[45] M. Ma, T. Mu, Modification of deoiled cumin dietary fiber with laccase and cellulase under high hydrostatic pressure, Carbohydr. Polym. 136 (2016) 87–94, https://doi.org/10.1016/J.CARBPOL.2015.09.030.
[46] F. Maestrelli, M. Garcia-Fuentes, P. Mura, M.J. Alonso, A new drug nanocarrier consisting of chitosan and hydoxypropylcyclodextrin, Eur. J. Pharm. Biopharm. 63 (2) (2006) 79–86, https://doi.org/10.1016/j.ejpb.2005.12.006.
[47] P.A. Magallanes-Cruz, P.C. Flores-Silva, L.A. Bello-Perez, Starch structure influences its digestibility: A Review, J. Food Sci. 82 (9) (2017) 2016–2023, https://doi.org/10.1111/1750-3841.13809.
[48] S.K. Mandal, R.P. Singh, V. Patel, Isolation and characterization of exopolysaccharide secreted by a toxic dinoflagellate, amphidinium carterae hulburt 1957 and its probable role in Harmful Algal Blooms (HABs), Microb. Ecol. 62 (3) (2011) 518–527, https://doi.org/10.1007/S00248-011-9852-5.
[49] J. Miao, J.M. Regenstein, J. Qiu, J. Zhang, X. Zhang, H. Li, H. Zhang, Z. Wang, Isolation, structural characterization and bioactivities of polysaccharides and its derivatives from Auricularia-A review, Int. J. Biol. Macromol. 150 (2020) 102–113, https://doi.org/10.1016/j.ijbiomac.2020.02.054.
[50] S. Miao, X. Mao, R. Pei, S. Miao, C. Xiang, Y. Lv, X. Yang, J. Sun, S. Jia, Y. Liu, Antitumor activity of polysaccharides from Lepista sordida against laryngocarcinoma in vitro and in vivo, Int. J. Biol. Macromol. 60 (2013) 235–240, https://doi.org/10.1016/J.IJBIOMAC.2013.05.033.
[51] J. Mo, J. Ni, M. Zhang, Y. Xu, Y. Li, N. Karim, W. Chen, Mulberry anthocyanins ameliorate dss-induced ulcerative colitis by improving intestinal barrier function and modulating gut microbiota, Antioxidants 11 (9) (2022), https://doi.org/10.3390/antiox11091674.
[52] T. Nakahari, Y. Sawabe, C. Shimamoto, Epithelial Transport of macromolecules: gastric mucous exocytosis, Membrane 36 (6) (2011) 286–292, https://doi.org/10.5360/membrane.36.286.
[53] L.S. Poritz, K.I. Garver, C. Green, L. Fitzpatrick, F. Ruggiero, W.A. Koltun, loss of the tight junction protein ZO-1 in dextran sulfate sodium induced colitis, J. Surg. Res. 140 (1) (2007) 12–19, https://doi.org/10.1016/j.jss.2006.07.050.
[54] Pujo, J., Petitfils, C., Le Faouder, P., Eeckhaut, V., Payros, G., Maurel, S., Perez-Berezo, T., Van Hul, M., Barreau, F., Blanpied, C., Chavanas, S., Van Immerseel, F., Bertrand-Michel, J., Oswald, E., Knauf, C., Dietrich, G., Cani, P. D., & Cenac, N. (2021). Bacteria-derived long chain fatty acid exhibits anti-inflammatory properties in colitis. Gut, 70(6), 1088 LP – 1097. https://doi.org/10.1136/gutjnl-2020-321173.
[55] Qiu, J., Zhang, H., & Wang, Z. (2019). Ultrasonic degradation of polysaccharides from Auricularia auricula and the antioxidant activity of their degradation products. Lwt, 113(March 2018), 108266. https://doi.org/10.1016/j.lwt.2019.108266.
[56] G. Ren, L. Xu, T. Lu, J. Yin, Structural characterization and antiviral activity of lentinan from Lentinus edodes mycelia against infectious hematopoietic necrosis virus, Int. J. Biol. Macromol. 115 (2018) 1202–1210, https://doi.org/10.1016/J.IJBIOMAC.2018.04.132.
[57] J.M. Rhodes, Colonic mucus and mucosal glycoproteins: the key to colitis and cancer? Gut 30 (12) (1989) 1660–1666, https://doi.org/10.1136/gut.30.12.1660.

[58] A. Roberti, L.E. Chaffey, D.R. Greaves, NF-κB Signaling and inflammation—drug repurposing to treat inflammatory disorders? Biology 11 (3) (2022) https://doi.org/10.3390/biology11030372.
[59] M. Rossol, H. Heine, U. Meusch, D. Quandt, C. Klein, M.J. Sweet, S. Hauschildt, LPS-induced cytokine production in human monocytes and macrophages, Critical Reviews™ in Immunology 31 (5) (2011) 379–446, https://doi.org/10.1615/CRITREVIMMUNOL.V31.I5.20.
[60] A. Ruda, A.H. Aytenfisu, T. Angles d'Ortoli, A.D. MacKerell, G. Widmalm, Glycosidic α-linked mannopyranose disaccharides: an NMR spectroscopy and molecular dynamics simulation study employing additive and Drude polarizable force fields, PCCP 25 (4) (2022) 3042–3060, https://doi.org/10.1039/d2cp05203b.
[61] Z. Sheng, J. Liu, B. Yang, Structure differences of water soluble polysaccharides in astragalus membranaceus induced by origin and their bioactivity, Foods 10 (8) (2021), https://doi.org/10.3390/foods10081755.
[62] A.C. Smith, D.K. Podolsky, Colonic mucin glycoproteins in health and disease, Clin. Gastroenterol. 15 (4) (1986) 815–837. http://europepmc.org/abstract/MED/3536210.
[63] K. Son Trinh, T. Linh Nguyen, C.M. City, H., Structural, functional properties and in vitro digestibiligy of maize starch under heat-moisture and atmospheric-cold plasma treatments, Vietnam Journal of Science and Technology 56 (6) (2018) 751–760. https://doi.org/10.15625/2525-2518/56/6/12357.
[64] G. Song, Q. Du, Structure characterization and antitumor activity of an α β-glucan polysaccharide from Auricularia polytricha, Food Res. Int. 45 (1) (2012) 381–387, https://doi.org/10.1016/J.FOODRES.2011.10.035.
[65] U. Surenjav, L. Zhang, X. Xu, X. Zhang, F. Zeng, Effects of molecular structure on antitumor activities of (1→3)-β-d-glucans from different Lentinus Edodes, Carbohydr. Polym. 63 (1) (2006) 97–104, https://doi.org/10.1016/J.CARBPOL.2005.08.011.
[66] A. Synytsya, K. Mickova, A. Synytsya, I. Jablonsky, J. Spevacek, V. Erban, E. Kovarikova, J. Copikova, Glucans from fruit bodies of cultivated mushrooms Pleurotus ostreatus and Pleurotus eryngii: Structure and potential prebiotic activity, Carbohydr. Polym. 76 (4) (2009) 548–556, https://doi.org/10.1016/j.carbpol.2008.11.021.
[67] Y. Tian, Y. Zhao, H. Zeng, Y. Zhang, B. Zheng, Structural characterization of a novel neutral polysaccharide from Lentinus giganteus and its antitumor activity through inducing apoptosis, Carbohydr. Polym. 154 (2016) 231–240, https://doi.org/10.1016/J.CARBPOL.2016.08.059.
[68] W. Tu, J. Zhu, S. Bi, D. Chen, L. Song, L. Wang, J. Zi, R. Yu, Isolation, characterization and bioactivities of a new polysaccharide from Annona squamosa and its sulfated derivative, Carbohydr. Polym. 152 (2016) 287–296, https://doi.org/10.1016/J.CARBPOL.2016.07.012.
[69] N. Vallianou, M. Dalamaga, T. Stratigou, I. Karampela, C. Tsigalou, Do Antibiotics cause obesity through long-term alterations in the gut microbiome? a review of current evidence, Curr. Obes. Rep. 10 (3) (2021) 244–262, https://doi.org/10.1007/s13679-021-00438-w.
[70] Vasilieva, T., Sigarev, A., Kosyakov, D., Ul'yanovskii, N., Anikeenko, E., Chuhchin, D., Ladesov, A., Hein, A. M., & Miasnikov, V. (2017). Formation of low molecular weight oligomers from chitin and chitosan stimulated by plasma-assisted processes. Carbohydrate Polymers, 163, 54–61. https://doi.org/10.1016/J.CARBPOL.2017.01.026.
[71] Z.-M. Wang, Y.-C. Cheung, P.-H. Leung, J.-Y. Wu, Ultrasonic treatment for improved solution properties of a high-molecular weight exopolysaccharide produced by a medicinal fungus, Bioresour. Technol. 101 (14) (2010) 5517–5522, https://doi.org/10.1016/j.biortech.2010.01.134.
[72] K.P. Williams, J.J. Gillespie, B.W.S. Sobral, E.K. Nordberg, E.E. Snyder, J. M. Shallom, A.W. Dickerman, Phylogeny of gammaproteobacteria, J. Bacteriol. 192 (9) (2010) 2305–2314, https://doi.org/10.1128/JB.01480-09.
[73] S.E. Winter, M.G. Winter, M.N. Xavier, P. Thiennimitr, V. Poon, A.M. Keestra, R. C. Laughlin, G. Gomez, J. Wu, S.D. Lawhon, I.E. Popova, S.J. Parikh, L.G. Adams, R.M. Tsolis, V.J. Stewart, A.J. Bäumler, Host-derived nitrate boosts growth of E. coli in the Inflamed Gut, Science 339 (6120) (2013) 708–711, https://doi.org/10.1126/science:1232467.
[74] D.T. Wu, Y. He, Q. Yuan, S. Wang, R.Y. Gan, Y.C. Hu, L. Zou, Effects of molecular weight and degree of branching on microbial fermentation characteristics of okra pectic-polysaccharide and its selective impact on gut microbial composition, Food Hydrocoll. 132 (2022) 107897, https://doi.org/10.1016/J.FOODHYD.2022.107897.
[75] J. Wu, H. Wang, Y. Liu, B. Xu, B. Du, Y. Yang, Effect of ultrasonic irradiation on the physicochemical and structural properties of Laminaria japonica polysaccharides and Their Performance in Biological Activities, Molecules 28 (1) (2023), https://doi.org/10.3390/molecules28010008.
[76] Xiao, H. T., Lin, C.-Y., H. H. Ho, D., Peng, J., Chen, Y., Tsang, S.-W., Wong, M., Zhang, X.-J., Zhang, M., & Bian, Z.-X., 2013. Inhibitory effect of the Gallotannin corilagin on dextran sulfate sodium-induced murine ulcerative colitis. Journal of Natural Products, 76(11), 2120–2125. https://doi.org/10.1021/np4006772.
[77] W. Xiong, Q. Zhang, F. Yin, S. Yu, T. Ye, W. Pan, X. Yang, Auricularia auricular polysaccharide-low molecular weight chitosan polyelectrolyte complex nanoparticles: Preparation and characterization, Asian J. Pharm. Sci. 11 (3) (2016) 439–448, https://doi.org/10.1016/j.ajps.2015.10.064.
[78] Y. Xu, Y. Guo, S. Duan, H. Wei, Y. Liu, L. Wang, X. Huo, Y. Yang, Effects of ultrasound irradiation on the characterization and bioactivities of the polysaccharide from blackcurrant fruits, Ultrason. Sonochem. 49 (2018) 206–214, https://doi.org/10.1016/j.ultsonch.2018.08.005.
[79] Yan, Y. xi, Shao, M. juan, Qi, Q., Xu, Y. sheng, Yang, X. qian, Zhu, F. hua, He, S. jun, He, P. lan, Feng, C. lan, Wu, Y. wei, Li, H., Tang, W., & Zuo, J. ping. (2018). Artemisinin analogue SM934 ameliorates DSS-induced mouse ulcerative colitis via suppressing neutrophils and macrophages. Acta Pharmacologica Sinica, 39(10), 1633–1644. https://doi.org/10.1038/aps.2017.185.
[80] Yu, J. S., Lim, S. H., Lee, S. R., Choi, C. I., & Kim, K. H. (2021). Antioxidant and anti-inflammatory effects of white mulberry (Morus alba L.) fruits on lipopolysaccharide-stimulated RAW 264.7 macrophages. Molecules 2021, Vol. 26, Page 920, 26(4), 920. https://doi.org/10.3390/MOLECULES26040920.
[81] D. Yuan, C. Li, Q. Huang, X. Fu, Ultrasonic degradation effects on the physicochemical, rheological and antioxidant properties of polysaccharide from Sargassum pallidum, Carbohydr. Polym. 239 (April) (2020) 116230, https://doi.org/10.1016/j.carbpol.2020.116230.
[82] L. Zhang, C. Fan, S. Liu, Z. Zang, L. Jiao, L. Zhang, Chemical composition and antitumor activity of polysaccharide from Inonotus obliquus, Journal of Medicinal Plants Research 5 (7) (2011) 1251–1260.
[83] M. Zhang, S.W. Cui, P.C.K. Cheung, Q. Wang, Antitumor polysaccharides from mushrooms: A review on their isolation process, structural characteristics and antitumor activity, Trends Food Sci. Technol. 18 (2007) 4–19.
[84] S. Zhang, Y. Cao, Y. Huang, S. Zhang, G. Wang, X. Fang, W. Bao, Aqueous M. oleifera leaf extract alleviates DSS-induced colitis in mice through suppression of inflammation, J. Ethnopharmacol. 318 (2024), https://doi.org/10.1016/j.jep.2023.116929.
[85] Z. Zhang, S. Li, H. Cao, P. Shen, J. Liu, Y. Fu, Y. Cao, N. Zhang, The protective role of phloretin against dextran sulfate sodium-induced ulcerative colitis in mice, Food Funct. 10 (1) (2019) 422–431, https://doi.org/10.1039/C8FO01699B.
[86] C. Zhao, C. Li, Q. Huang, X. Fu, Characterization, functional and biological properties of degraded polysaccharides from Hylocereus undatus flowers, J. Food Process. Preserv. 43 (7) (2019) e13973, https://doi.org/10.1111/JFPP.13973.
[87] Zhu, L., Lu, Y., Sun, Z., Han, J., & Tan, Z. (2020). The application of an aqueous two-phase system combined with ultrasonic cell disruption extraction and HPLC in the simultaneous separation and analysis of solanine and Solanum nigrum polysaccharide from Solanum nigrum unripe fruit. Food Chemistry, 304(September 2018). https://doi.org/10.1016/j.foodchem.2019.125383.
[88] W. Zhu, M.G. Winter, M.X. Byndloss, L. Spiga, B.A. Duerkop, E.R. Hughes, L. Büttner, E. de Lima Romão, C.L. Behrendt, C.A. Lopez, L. Sifuentes-Dominguez, K. Huff-Hardy, R.P. Wilson, C.C. Gillis, Ç. Tükel, A.Y. Koh, E. Burstein, L.V. Hooper, A.J. Bäumler, S.E. Winter, Precision editing of the gut microbiota ameliorates colitis, Nature 553 (7687) (2018) 208–211, https://doi.org/10.1038/nature25172.